

# The evolution of cloud and aerosol microphysics at the summit of Mt. Tai, China

Jiarong Li<sup>1</sup>, Chao Zhu<sup>1</sup>, Hui Chen<sup>1,\*</sup>, Defeng Zhao<sup>1</sup>, Likun Xue<sup>2</sup>, Xinfeng Wang<sup>2</sup>, Hongyong Li<sup>2</sup>, Pengfei Liu<sup>3,4,5</sup>, Junfeng Liu<sup>3,4,5</sup>, Chenglong Zhang<sup>3,4,5</sup>, Yujing Mu<sup>3,4,5</sup>, Wenjin Zhang<sup>6</sup>, Luming Zhang<sup>7</sup>, Kai Li<sup>7</sup>, Min Liu<sup>7</sup>, Hartmut Herrmann<sup>1,2,8</sup>, Jianmin Chen<sup>1,4,9,\*</sup>

<sup>1</sup>Shanghai Key Laboratory of Atmospheric Particle Pollution and Prevention (LAP3), Department of Environmental Science and Engineering, Institute of Atmospheric Sciences, Fudan University, Shanghai 200438, China

<sup>2</sup>Environment Research Institute, School of Environmental Science and Engineering, Shandong University, Ji'nan 250100, China

<sup>3</sup>Research Center for Eco-Environmental Science, Chinese Academy of Sciences, Beijing 10085, China

<sup>4</sup>Center for Excellence in Urban Atmospheric Environment, Institute of Urban Environment, Chinese Academy of Science, Xiamen 361021, China

<sup>5</sup>University of Chinese Academy of Sciences, Beijing 100049, China

<sup>6</sup>State Environmental Protection Key Laboratory of Urban Ambient Air Particulate Matter Pollution Prevention and Control, College of Environmental Science and Engineering, Nankai University, Tianjin 300071, China

<sup>7</sup>Tai'an Municipal Ecological Environment Bureau, Shandong Tai'an Ecological Environment Monitoring Center, Tai'an 271000, China

<sup>8</sup>Leibniz Institute for Tropospheric Research, Leipzig, Germany

<sup>9</sup>Shanghai Institute of Eco-Chongming (SIEC), No.3663 Northern Zhongshan Road, Shanghai 200062, China

*Corresponding to:* Jianmin Chen (jmchen@fudan.edu.cn) and Hui Chen (hui\_chen@fudan.edu.cn)

**Abstract.** The influence of aerosols, both natural and anthropogenic, remains a major area of uncertainty when predicting the properties and the behaviours of clouds and their influence on climate. In an attempt to understand better the microphysical properties of cloud droplets, simultaneous variations in aerosol microphysics and their potential interactions during cloud life cycles in the North China Plain, an intensive observation took place from 17 June to 30 July 2018 at the summit of Mt. Tai. Cloud microphysical parameters were monitored simultaneously with number concentrations of cloud condensation nuclei ( $N_{CCN}$ ) at different supersaturations,  $PM_{2.5}$  mass concentrations, particle size distributions and meteorological parameters. Number concentrations of cloud droplets ( $N_C$ ), liquid water content ( $LWC$ ) and effective radius of cloud droplets ( $r_{eff}$ ) show large variations among 40 cloud events observed during the campaign. The low values of  $r_{eff}$  and  $LWC$  observed at Mt. Tai are comparable with urban fogs. Clouds in clean days are more susceptible to the change in concentrations of particle number ( $N_P$ ), while clouds formed in polluted days might be more sensitive to meteorological parameters such as updraft velocity and cloud base height. Through studying the size distributions of aerosol particles and cloud droplets, particles larger than 150 nm play important roles on forming cloud droplets with the size of 5–10  $\mu m$ . In general,  $LWC$  consistently varies with  $r_{eff}$ . As  $N_C$  increases,  $r_{eff}$  changes from a trimodal distribution to a unimodal distribution and shifts to smaller size mode. By assuming a constant cloud thickness and tanking no account of the cloud lifetime, increase in  $N_C$  and decrease in  $r_{eff}$  would increase cloud albedo, which may induce a cooling effect on the local climate system. Our results contribute valuable information to enhance

1 the understanding on cloud and aerosol properties along with their potential interactions in North China plain.

## 2 1. Introduction

3 Clouds are key factors in the atmospheric hydrological cycle, which play an important role in the atmospheric energy  
4 budget and significantly influence the global and regional climate (Chang et al., 2019;Zhang et al., 2004b). Clouds can be  
5 physically described by their liquid water contents ( $LWC$ ), number concentrations of droplets ( $N_C$ ) and effective radius of  
6 droplets ( $r_{eff}$ ). These parameters may show small inter-annual variations for the same monitoring station (Möller et al., 1996),  
7 but they would vary over a large range for different cloud types (Quante, 2004), for different cloud altitudes (Padmakumari et  
8 al., 2017;Zhao et al., 2018) and in different parts of a cloud (Deng et al., 2009).

9 The interactions between the clouds and the aerosols are complex. Clouds can efficiently remove aerosols by activating  
10 CCN to cloud droplets (Croft et al., 2010;Zhang et al., 2004a). The cloud processes can incorporate large amount of fine  
11 particulate mass (Heintzenberg et al., 1989), change their size distributions (Drewnick et al., 2007;Schroder et al., 2015) and  
12 alter the CCN compositions through homogeneous and heterogeneous reactions (Roth et al., 2016). In addition, the variation  
13 of aerosol number concentrations and aerosol size distributions could alter the cloud microphysics. Through studying  
14 microphysical characteristics of cloud droplet residuals at Mt. Åreskutan, Noone et al. (1990) found that larger cloud droplets  
15 preferred to form on larger Cloud Condensation Nuclei (CCN). What's more, the aerosol-cloud interaction has been  
16 investigated for cloud processes formed under both clean and polluted conditions. Padmakumari et al. (2017) found that  
17 convective clouds over land were characterized by lower  $LWC$  and higher  $N_C$  due to the increase of pollution aerosol. Ground-  
18 based observations by radiometers during the summers of the U.S. Studies in mid-Atlantic region revealed that cloud events  
19 with smaller droplets ( $< 7 \mu m$ ) were more frequently observed in the polluted years than in the clean years (Li et al., 2017b).  
20 The influence of aerosols on the cloud microphysics is evident but varies for different regions and for different cloud types.

21 For a given liquid water content, aerosol particles can act as CCN, lead to higher number concentrations of cloud droplets  
22 with smaller sizes and result in higher albedo (Twomey effect or first indirect effect, FIE) (Twomey, 1974). Based on the  
23 principle of Twomey effect, calculations for evaluating the influence of aerosols on the cloud microphysics have been widely  
24 studied (Lohmann and Feichter, 2005;McComiskey et al., 2009;Twohy et al., 2005). However, arithmetic terms representing  
25 aerosol loading are different, such as using the number concentration of particles, the CCN concentration and the aerosol  
26 optical depth (AOD), which makes it difficult to compare the FIE from different studies.

27 The increase in the aerosol concentrations can result in a longer cloud lifetime, thus producing large cloud fractions  
28 (Koren et al., 2005;Albrecht, 1989), increasing cloud top height, and increasing the cloud thickness (Fan et al., 2013). It would  
29 further influence the regional and global climate (Rosenfeld, 2006;Seinfeld et al., 2016), such as reducing the precipitation or  
30 drizzle (Andreae et al., 2004;Heikenfeld et al., 2019) and further delaying the hydrological cycle (Rosenfeld, 2006). Through

1 Model experiments with the Coupled Model Intercomparison Project phase 5 (CMIP5), Frey et al. (2017) also found that the  
2 addition of anthropogenic aerosols could increase the monthly mean cloud albedo of subtropical marine stratocumulus clouds.

3 In situ measurements of cloud microphysics by aircraft or on high-altitude monitoring sites have provided some additional  
4 information for insight into the cloud processes (Allan et al., 2008; Li et al., 2017a; Padmakumari et al., 2017; Van Pinxteren et  
5 al., 2016; Reid et al., 1999). However, lacking knowledge of the size distributions of cloud droplets and aerosol particles makes  
6 it difficult to evaluate the cloud microphysics in small-scale regions (Fan et al., 2016; Khain et al., 2015; Sant et al., 2013).  
7 Discrepancy still exists between the widths of observed and simulated size distributions of cloud droplets (Grabowski and  
8 Wang, 2013). What's more, incompletely knowledge of the impact of cloud-aerosol interactions (Rosenfeld et al., 2014b),  
9 unresolved process of cloud formation (Stevens and Bony, 2013) and the lack of researches about the variation of cloud  
10 microphysical parameters at different cloud stages still hinder modelling studies.

11 In the study, in situ observations at the summit of Mt. Tai were presented to investigate the evolution of cloud microphysics  
12 coupled to simultaneous monitoring of aerosol size distributions,  $PM_{2.5}$  mass and CCN concentrations within non-precipitating  
13 clouds. The summit of Mt. Tai is the highest point in the centre of the North China Plain (NCP). Sufficient moisture in summer  
14 and dramatic temperature differences between day and night make it ideal for in situ orographic cloud monitoring (Li et al.,  
15 2017a). The summit of Mt. Tai is far away from anthropogenic emission sources on the ground. But high concentrations of  
16 inorganic ions in  $PM_{2.5}$  (Zhou et al., 2009), abundant bacterial communities (Zhu et al., 2018),  $NH_3$  and  $NO_x$  emissions from  
17 biomass burning (Chang et al., 2018) have been observed at the summit, thus a strong anthropogenic influence is existing.  
18 Previous studies of cloud samples collected at the same position showed high inorganic ion concentrations (Li et al.,  
19 2017a; Wang et al., 2011), which can be attributable to the increase of anthropogenic aerosol. In the present study, two typical  
20 cloud processes are discussed in detail to elucidate the relationship of  $N_C$ ,  $r_{eff}$  and  $LWC$  under clean or polluted conditions  
21 (indicated by  $N_P$  and  $N_{CCN}$ ) and during the cloud life cycle. The present paper provides comprehensive information of cloud  
22 microphysical properties and their potential links to aerosol concentrations and size distribution. Implications of cloud and  
23 aerosol microphysics for cloud albedo and climate are discussed.

## 24 2. Experiments

### 25 2.1. Observation duration and site

26 From 17 June to 30 July 2018, 40 cloud events in total were monitored at the Shandong Taishan Meteorological Station at  
27 summit of Mt. Tai (Tai'an, China;  $117^{\circ}13'$  E,  $36^{\circ}18'$  N; 1545 m a.s.l.; Fig. S1). Mt. Tai is the highest point in the central of  
28 North China Plain (NCP) and located within the transportation channel between the NCP and the Yangtze River Delta (Shen  
29 et al., 2019). The altitude of Mt. Tai is close to 1.6 km. This height is close to the top of the planetary boundary layer in Central  
30 East China and usually sited for the characteristic of particles inputting to clouds (Hudson, 2007). Orographic clouds, which

are mainly formed in the boundary layer as air approaching the ridge, forced to rise up and cooled by adiabatic expansion (Choularton et al., 1997), frequently occur at the summit of Mt. Tai, especially in summer. Previous studies concentrated on cloud chemistry presented Mt. Tai is significantly influenced by anthropogenic emissions (Li et al., 2017a; Wang et al., 2011). In addition, fixed observation location is mainly applied to study the evolution of aerosol properties and cloud processing (Mertes et al., 2005; Roth et al., 2016). Thus, Mt. Tai is a good site for monitoring orographic clouds and simultaneously investigating aerosol and cloud microphysics. The arrangement of instruments was presented in Fig. S1(c). As shown in Fig. S2, the prevailing wind direction during this summer campaign is east wind (23.3%), southwest wind (22.8%) and south wind (21.9%), respectively. About 85.6% of wind speed was less than 8 m s<sup>-1</sup>. While the monitored cloud events in the present study was mainly influence by south wind (34.7%) and southwest wind (22%).

## 2.2. Cloud microphysical parameters

A Fog Monitor (Model FM-120, Droplet Measurement Technologies Inc., USA), a forward-scattering optical spectrometer with sampling flow of 1 m<sup>3</sup> min<sup>-1</sup>, was applied in situ for real-time displaying size distributions of cloud droplets and computing  $N_C$ ,  $LWC$ , median volume diameter ( $MVD$ ) and effective diameter ( $ED$ ) in the size range of 2 to 50 μm (Spiegel et al., 2012). The corresponding equations are:

$$N_C = \sum N_i,$$

$$LWC = \frac{4\pi}{3} \sum N_i r_i^3 \rho_w,$$

$$MVD = 2 \times \left( \frac{\sum N_i r_i^3}{\sum N_i} \right)^{\frac{1}{3}}$$

$$ED = 2 \times r_{eff} = 2 \times \sum n_i r_i^3 / \sum n_i r_i^2,$$

Where  $N_i$  is the cloud number concentration at the  $i^{th}$  bin,  $r_i$  represents the radius at the  $i^{th}$  bin and  $\rho_w = 1$  g cm<sup>-3</sup> stands for the density of liquid water. Droplets are categorized into manufacture's predefined 30 size bins with sampling resolution of 1 s. The size bin widths using this configuration were 1 μm for droplets < 15 μm and 2 μm for droplets > 15 μm. The true air speed calibration and size distribution calibration of FM-120 were carried out by the manufacturer using borosilicate glass microspheres of various sizes (5.0, 8.0, 15.0, 30.0, 40.0 and 50.0 μm, Duke Scientific Corporation, USA). The difference in optical properties between the glass beads and water was taken into account during the calibration process. In this study, the sampling inlet nozzle faced the main wind direction and was horizontally set. Cloud events are defined by the universally accepted threshold values in  $N_C$  and  $LWC$ , i.e.,  $N_C > 10$  # cm<sup>-3</sup> and  $LWC > 0.001$  g m<sup>-3</sup> (Demos et al., 1996). Too short cloud events with a duration < 15 minutes were excluded.

## 2.3. Aerosol size distribution

A Scanning Mobility Particle Sizer (SMPS, Model 3938, TSI Inc., USA) consisting of a Differential Mobility Analyzer (DMA,

Model 3082, TSI Inc., USA) and a Condensation Particle Counter (CPC, Model 3775, TSI Inc., USA) was applied to monitor the size distributions of dehumidified aerosols through a PM<sub>10</sub> inlet. The neutralized aerosols were classified by DMA to generate a monodisperse stream of known size according to their electrical mobility. The CPC placed downstream counts the particles and gives the number of particles with different sizes. In the present study, each scan was fixed at 5 min for every loop with a flow rate of 1.5 L min<sup>-1</sup> sizing particles in the range of 13.6 – 763.5 nm in 110 size bins.

#### 2.4. CCN number concentration

The  $N_{CCN}$  at certain supersaturations ( $SS$ ) were quantified by a Cloud Condensation Nuclei Counter (Model CCN-100, DMT Inc., USA). The CCN counter was set at five  $SS$  values sequentially for 10 min each at 0.2 %, 0.4 %, 0.6 %, 0.8 % and 1.0 % with a full scan time resolution of 50 min. Data collected during the first 5 min of each  $SS$  was excluded since the CCN counter needs time for temperature stabilization after the change of  $SS$ . The ratio of sample flow to sheath flow was set at 1:10 with a total airflow of 500 ccm. The  $SS$  of CCN counter were calibrated before the campaign and checked at the end of the campaign with monodisperse ammonium sulfate particles of different sizes (Rose et al., 2008).

#### 2.5. PM<sub>2.5</sub> concentrations and meteorological parameters

The PM<sub>2.5</sub> mass concentration was measured using a beta attenuation and optical analyzer (SHARP monitor, model 5030i, Thermo Scientific Inc., USA). Meteorological parameters including the ambient temperature ( $T_a$ , °C), relative humidity ( $RH$ ), wind speed ( $WS$ , m s<sup>-1</sup>) and wind direction ( $WD$ , °) were provided by Shandong Taishan Meteorological Station at the same observation point. The ground-level temperature ( $T_g$ ), ground-level pressure ( $P_g$ ), and dew point temperature ( $T_{gd}$ ) were supported by National Meteorological Observatory – Tai'an Station (station number: 54827, 117°9' E, 36°9' N, 128.6 m a.s.l) (Fig. S1(a)), which sited in the south plain of Mt. Tai.

#### 2.6. Calculation of cloud base height

In the present study, the estimated lifting condensation level ( $LCL$ ) is applied to represent the cloud base height ( $CBH$ ) due to the lack of corresponding instruments. The calculation of  $LCL$  depends on the meteorological parameters measured at Tai'an Station. The ground-level data of temperature, dew point temperature, and pressure were used as input parameters (Georgakakos and Bras, 1984):

$$p_{LCL} = \frac{1}{\left(\frac{T_g - T_{gd}}{223.15} + 1\right)^{3.5}} \times p_g$$

$$T_{LCL} = \frac{1}{\left(\frac{T_g - T_{gd}}{223.15} + 1\right)} \times T_g$$

$$CBH = 18400 \times \left(1 + \frac{T_{LCL} - T_g}{273}\right) \times \lg \frac{p_g}{p_{LCL}}$$

1 Where  $p_{LCL}$  is the *LCL* pressure;  $T_{LCL}$  is the *LCL* temperature.

## 2 **2.7. Calculation of AIE**

3 Aerosol indirect effect (AIE), which **here** represents simply approximations of the derivatives of the cloud microphysics ( $r_{eff}$   
4 and  $N_C$ ) with respect to changes in aerosol concentrations (McComiskey et al., 2009;Feingold et al., 2001), is applied to study  
5 the influence of  $N_P$  on cloud microphysics and calculated as:

$$6 \quad AIE_r = -\left(\frac{\Delta \ln r_{eff}}{\Delta \ln N_P}\right)_{LWC}, 0 < AIE_r < 0.33$$

$$7 \quad AIE_N = \left(\frac{\Delta \ln N_C}{\Delta \ln N_P}\right), 0 < AIE_N < 1$$

8 Where  $N_P$  is applied as an proxy of aerosol amount (Zhao et al., 2012;Zhao et al., 2018).

## 9 **2.8. Calculation of cloud albedo**

10 Cloud albedos can be calculated using the equations shown below (Seinfeld and Pandis, 2006). Assuming the cloud droplet  
11 size distribution can be approximated as monodisperse and the cloud is vertically uniform with respect to droplet size  
12 distribution (Stephens, 1978), the cloud optical thickness ( $\tau_c$ ) could be obtained by:

$$13 \quad \tau_c = h \left( \frac{9\pi LWC^2 N_C}{2\rho_w^2} \right)^{\frac{1}{3}}$$

14 Where  $h$  is the thickness of the cloud and  $\rho_w$  is the density of cloud water.

15 For the nonabsorbing and horizontally homogeneous cloud, the two-stream approximation for the cloud albedo ( $R_c$ ) gives  
16 as (Lacis and Hansen, 1974):

$$17 \quad Albedo = \frac{\sqrt{3}(1-g)\tau_c}{2 + \sqrt{3}(1-g)\tau_c}$$

18 Where  $g$  is the asymmetry factor. The radius of cloud droplets was much greater than the wavelength of visible light, hence  $g$   
19 is 0.85. The equation before becomes to:

$$20 \quad Albedo = \frac{\tau_c}{\tau_c + 7.7}$$

## 21 **3. Results and discussion**

### 22 **3.1. Overview of the cloud microphysics**

23 During 17<sup>th</sup> June to 30<sup>th</sup> July 2018, 40 cloud events were captured at the summit of Mt. Tai. Large ranges of cloud  
24 microphysics have been observed during the campaign. The averaged  $N_C$ ,  $LWC$ , and  $r_{eff}$  of the 40 cloud events at the summit  
25 of Mt. Tai varied over the ranges of 59–1519 # cm<sup>-3</sup>, 0.01–0.59 g m<sup>-3</sup> and 2.6–7.4 μm, respectively (Table S1). The monitored  
26 number concentration of cloud droplets at Mt. Tai both in the present study and in 2014 can reach 2000–3000 # cm<sup>-3</sup> (Li et al.,  
27 2017a), which is much higher than those values (with a range of 10–700 # cm<sup>-3</sup>) for city fogs and convective and orographic

1 clouds (Allan et al., 2008; Li et al., 2011; Padmakumari et al., 2017) (Table 1). It represented clouds at Mt. Tai were characterized  
2 with high  $N_C$ .

3 The microphysics of different clouds and fogs can generally be distinguished in a plot of  $r_{eff}$  (or  $MVD$ ) against  $LWC$ . As  
4 illustrated in Fig. 1, the  $LWC$  generally increases in order of city fogs, orographic clouds and convective clouds, and Mt. Tai  
5 generally follows this rule. It is consistent with the study by Penner et al. (2004) that  $LWC$  within clouds increases linearly  
6 with altitude. For  $LWC$  values of clouds at Mt. Tai, we monitored the high values, which are comparable with convective  
7 clouds, and the low values, which are similar to city fogs (Fig. 1). It indicated that clouds at Mt. Tai appeared to show a larger  
8 range of  $LWC$  values. The increase of  $LWC$  at Mt. Tai should be determined by the increase of  $r_{eff}$  and/or  $N_C$ . But sometimes  
9 only one factor plays the determining role. As illustrated in Table S1,  $N_C$ ,  $r_{eff}$  and  $LWC$  in cloud event 20 (CE-20) were 1519  
10  $\# \text{ cm}^{-3}$ ,  $5.2 \mu\text{m}$  and  $0.54 \text{ g m}^{-3}$ , respectively, while the corresponding values in cloud event 16 (CE-16) were 59  $\# \text{ cm}^{-3}$ ,  $9.8 \mu\text{m}$   
11 and  $0.14 \text{ g m}^{-3}$ , respectively. Even though  $r_{eff}$  of CE-20 was smaller compared with CE-16, but the higher  $N_C$  determined the  
12 larger  $LWC$  of clouds in CE-20. In the following parts, the evolution of cloud and aerosol microphysical properties were  
13 presented. The influence of meteorological parameters (such as updraft velocity and cloud base height) and aerosol particle on  
14 cloud microphysics were discussed.

### 15 3.2. Analysis on typical cloud processes

16 By assuming a density of  $\rho = 1.58 \text{ g cm}^{-3}$  (Cross et al., 2007), the mass concentrations of particles, which were calculated  
17 from the aerosol number size distribution measured by SMPS and named as  $\text{PM}_{0.8}$ , was highly consistent with  $\text{PM}_{2.5}$ , especially  
18 when  $\text{PM}_{2.5}$  was less than  $20 \mu\text{g m}^{-3}$  (Fig. 2(c)). Based on the mass concentration ( $\text{PM}_{2.5}$ ) and the number concentration ( $N_P$ ,  
19 which represented the total number concentration of aerosol particles measured by SMPS) of aerosols, two typical cloud  
20 processes, cloud process-1 (CP-1) and cloud process-2 (CP-2), were selected and analysed with their special characteristics.  
21 The influence of topography and updraft velocity ( $v_{up}$ ) on Fog Monitor during CP-1 and CP-2 could be ignored. The detailed  
22 information could be found in the Supplement (Table S2, Fig. S3 and Fig. S4) and was briefly introduced here. The sampling  
23 angle ( $\theta_s$ ) and  $v_{up}$  for CP-1 and CP-2 were  $11.9^\circ$  and  $0.82 \pm 0.29 \text{ m s}^{-1}$ , and  $10.6^\circ$  and  $0.92 \pm 0.36 \text{ m s}^{-1}$ , respectively (Table  
24 S2). According to the calculations provided by (Spiegel et al., 2012), the aspiration efficiency and transmission efficiency were  
25 all close to 1. In CP-1 (contained only cloud event 19 (CE-19)), cloud droplets formed under a relatively stable (wind speed  $<$   
26  $4 \text{ m s}^{-1}$ ) and clean ( $\text{PM}_{2.5} \approx 10.9 \mu\text{g m}^{-3}$ ,  $N_P \approx 1425 \# \text{ cm}^{-3}$ ) conditions accompanied by a slow increase of  $T_a$  (Fig. 2 and Fig.  
27 3). During daytime, especially in the afternoon, the  $\text{PM}_{2.5}$  mass concentration dramatically increased with few changes in wind  
28 speed and wind direction, meanwhile,  $N_P$  reached to about  $5000 \# \text{ cm}^{-3}$  (Fig. 3). CP-1 persisted for 74 h, making it the longest  
29 cloud event during the present campaign. Quite different from CP-1, CP-2 contained eight cloud events (CE-20 to cloud event  
30 26 (CE-26), Fig. 3) and occurred periodically under high  $\text{PM}_{2.5}$  (Fig. 2,  $50.7 \mu\text{g m}^{-3}$  in average) as well as high  $N_P$  (Fig. 3,  $1694$   
31  $\# \text{ cm}^{-3}$  in average) conditions. Cloud events in CP-2 formed after sunset with sharp decreasing of  $\text{PM}_{2.5}$  and  $N_P$ , and transitorily



1 dissipated at noon accompanied with the increase of  $PM_{2.5}$ ,  $N_P$ ,  $T_a$  and cloud base height ( $CBH$ ). For cloud water samples  
2 collected during CP-1 and CP-2, the percentage of chemical compositions did not change a lot (Fig. S5). Three dominant main  
3 anions (sulfate, nitrate and ammonia) accounted for 93.39% in CP-1 and 90.37% in CP-2 of the total measured ions. The high  
4 concentration of secondary ions in the cloud water samples indicated that clouds at Mt. Tai were dramatically influenced by  
5 anthropogenic emissions.

6 CP-1 was separated into four stages, including SL1 (stage-low 1), SH1 (stage-high 1), SL2 (stage-low 2), and SH2 (stage-  
7 high 2) based on the aerosol concentrations (Fig. 3). The characteristics of SL1 and SL2 were low  $N_C$  (383 and 347 #  $cm^{-3}$ ,  
8 respectively), large  $r_{eff}$  (7.26 and 6.36  $\mu m$ , respectively) and high  $LWC/N_C$  (1.01 and 0.75  $ng \#^{-1}$ , respectively, which represents  
9 averaged water each cloud droplet contained). During SH1 and SH2, dramatic increase of  $N_C$  (to 949 and 847 #  $cm^{-3}$ ,  
10 respectively), decrease of  $r_{eff}$  (to 4.90 and 4.88  $\mu m$ , respectively), and decrease of  $LWC/N_C$  (to 0.35 and 0.36  $ng \#^{-1}$ , respectively)  
11 occurred with the increase of  $N_P$  (to 4196 and 4665 #  $cm^{-3}$ , respectively).

12 Each cloud event of CP-2 was separated into activation stage (S1), collision-coalescence stage (S2), stable stage (S3),  
13 and dissipation stage (S4) according to the regular changes of  $N_C$  and  $LWC/N_C$  (Fig. 3(a)). In S1,  $N_C$  dramatically increased to  
14 its maximum value among the cloud events. In S2,  $N_C$  declined sharply to a stable value, meanwhile  $LWC/N_C$  reached the  
15 maximum value. In S3,  $N_C$  was stable or slightly varied and  $LWC/N_C$  started to decrease. In S4, both  $N_C$  and  $LWC/N_C$  decreased  
16 sharply again and finally arrived zero. Even though the two stages (S2 and S3) in cloud event 25 (CE-25) were not totally  
17 follow the division rules, the other six cloud events followed well. It indicated that the division was helpful to study the  
18 variations of cloud microphysical properties during CP-2. The newly formed cloud droplets during S1 were characterized by  
19 small size, high  $N_C$  and low  $LWC/N_C$  values (Fig. 2(f) and 3(b)). For example, about 2310 #  $cm^{-3}$  of cloud droplets can quickly  
20 form in the first 2 hours of CE-20. The  $r_{eff}$  of these droplets was smaller than 4.1  $\mu m$  and  $LWC/N_C$  was about 0.2  $ng \#^{-1}$ . In  
21 going from S2 to S3, the strong collision-coalescence between cloud droplets caused the increase of both  $r_{eff}$  and  $LWC/N_C$ . In  
22 S4, the increase of  $PM_{2.5}$ , through evaporation of cloud droplets or lifting of  $CBH$  (Fig. 2), was observed to coincide with the  
23 vanishment of cloud events (Mazoyer et al., 2019; Li et al., 2017a).

### 24 3.2.1. Relationships among $N_P$ , $N_{CCN}$ and $N_C$

25 In the present study, both consistent variation and inverse variation between  $N_P$  and  $N_C$  were observed.  $N_P$  and  $N_C$  showed  
26 consistent variation in CP-1. But in CP-2, an obviously inverse variation was found between  $N_P$  and  $N_C$  in S1 and S4, while a  
27 simultaneously variation was found between  $N_P$  and  $N_C$  in S2 and S3 (Fig. 3(a), Fig. 4(b), and Fig. 4(c)). Some in situ  
28 observations (Lu et al., 2007; Mazoyer et al., 2019) and modelling studies (Heikenfeld et al., 2019; Zhang et al., 2014) supported  
29 the viewpoint that the increase of  $N_P$  brings more CCN and further increases  $N_C$ , which caused the consistent variation between  
30  $N_P$  and  $N_C$ . In contrast, some recent studies of fogs also suggested that the increase of  $N_P$  would decrease the ambient  
31 supersaturation and then decrease  $N_C$  (Boutle et al., 2018; Mazoyer et al., 2019). Besides, Modini et al. (2015) found inverse



1 variation between  $N_C$  and the number of particles with diameters larger than 100 nm due to the reduction of supersaturation by  
 2 coarse primary marine aerosol particles. In general, the covariation between  $N_P$  and  $N_C$  could be affected by many factors,  
 3 including competition of water vapor between aerosol particles and/or cloud droplets, the scavenging of particles by cloud  
 4 droplets, and new particles formation through cloud processes. In the present study, consistent variation between  $N_P$  and  $N_C$   
 5 was characterized with higher  $LWC/N_C$ , while inverse variation between  $N_P$  and  $N_C$  was appeared with lower  $LWC/N_C$ . The  
 6 averaged  $LWC/N_C$  was 0.61 ng #<sup>-1</sup> in CP-1 and were 0.15, 0.42, 0.39, 0.16 ng #<sup>-1</sup> in S1, S2, S3, S4, respectively, in CP-2.  
 7 Relative higher  $LWC/N_C$  value indicating water was sufficient for new cloud droplet formation. Once  $N_P$  increased, part of the  
 8 cloud water was taken away by the CCN in the particles to form new droplets, and the remaining amount of water was still  
 9 sufficient to maintain the previous droplets in liquid state. Thus, both  $N_P$  and  $N_C$  simultaneously increased. On the other hand,  
 10 relative lower  $LWC/N_C$  values, to some extent, could limit the formation of new cloud droplets. The activated particles grew  
 11 at the beginning of the cloud cycle would lower the surrounding supersaturation and to some extent limit further aerosol  
 12 activation (Ekman et al., 2011). The part of water taken by the CCN in the particles was not enough to active all of them to be  
 13 new droplets and the remaining amount of water was also insufficient to maintain all the previous droplets in liquid state. Then  
 14 the  $N_C$  would decrease and the more the  $N_P$ , the sharper decrease the  $N_C$  would be. Thus, the inverse variation between  $N_P$  and  
 15  $N_C$  could be observed.

16 The ratio between  $N_{CCN}$  and  $N_P$  could reflect the activation ratio of aerosol particles. As shown in Fig. S6,  $N_{CCN}$  increased  
 17 with the increase of SS. In addition,  $N_{CCN}$  of CP-2 was higher than that of CP-1 at the same SS. In order to compare with  
 18 previous studies as discussed below, SS = 0.2 % was chosen to calculate  $N_{CCN}/N_P$ , which represented the activation ratio of  
 19 aerosol particles. As shown in Fig. 3(b),  $N_{CCN,0.2}/N_P$  (activation ratio at a certain SS = 0.2 %) ranged from 0.06 to 0.69 in CP-1  
 20 yet it was range from 0.22 to 0.66 in CP-2. The averaged value of 0.30 in CP-1 was smaller than that of 0.38 in CP-2 and  
 21 values lower than 0.22 did not appear during CP-2. It indicated that the activation of aerosol particles in CP-2 was relatively  
 22 easier. Both the size distribution and the chemical composition could impact the cloud-nucleating ability of aerosol particles  
 23 (Dusek et al., 2006; Mazoyer et al., 2019). In order to discuss the activation ratio with aerosol size, Fig. S7 showed the relation  
 24 between  $N_{CCN,0.2}/N_P$  with  $GMr_P$  during CP-1 and CP-2. As can be seen, the higher correlation of  $N_{CCN,0.2}/N_P$  with  $GMr_P$  was  
 25 found during CP-1 than during CP-2, which represented the physical properties might have more influence on the activation  
 26 of aerosols during CP-1. Besides, Asmi et al. (2012) found that higher  $N_{CCN}/N_P$  and more concentrated plot of  $N_{CCN}$  versus  $N_P$   
 27 were usually occurred during winter when higher fraction of aged organics was observed during the observation program at  
 28 Puy-de-Dome, France. In this study, the plot of  $N_{CCN,0.2}$  versus  $N_P$  was found more scatter in CP-1 than that in CP-2 (Fig. S8).  
 29 Even though the settled SS in the present study (SS = 0.2%) is different from that at puy-de-Dome (SS = 0.24%), most of the  
 30 data points of CP-1 and CP-2 distributed between the two recommended dashed lines (the visually defined boundaries in within  
 31 most of the data are centered, Fig. S8) by Asmi et al. (2012). It suggested that the difference of aerosol organic chemical

1 compositions during CP-1 and CP-2 might also a reason for explaining the different activation ratio of aerosol particles during  
2 these two cloud processes.

### 3 **3.2.2. The influence of $N_p$ , $CBH$ and $v_{up}$ on Cloud Microphysics**

4 No negative  $AIE_r$  nor  $AIE_N$  were found in the present study (Fig. 4). The positive  $AIE_r$  and  $AIE_N$  at Mt. Tai mean that the  
5 increase in  $N_p$  are accompanied by decreased  $r_{eff}$  and increased  $N_C$ . But in the studies of Yuan et al. (2008) and Tang et al.  
6 (2014), AOD was applied to represent aerosol loading and negative  $AIE_r$  (indicating  $r_{eff}$  increased with the increasing of AOD)  
7 near coastlines of the Gulf of Mexico, the South China Sea and over Eastern China with the surrounding sea was found. The  
8 reason proposed by Yuan et al. (2008) was the increasing slightly soluble organics (SSO) particles, which would increase the  
9 critical supersaturation and hinder the activation of the particles. Meanwhile, Tang et al. (2014) represented that the  
10 meteorological conditions, which favoured the transportation of pollutants and water vapour, led to simultaneous increases in  
11 both AOD and  $r_{eff}$ . Different from the coastal area, the summit of Mt. Tai is relatively far from the sea (around 230 km from  
12 the Bohai Sea and Yellow Sea) (Guo et al., 2012), making the less moist in the air. It might hinder the growth of cloud droplets  
13 and caused the positive  $AIE_r$ . In addition, the increase in  $LWC$  was found covariance with the decrease of  $AIE$ , especially at  
14 coastal sites (McComiskey et al., 2009; Zhao et al., 2012). But, non-obvious variation was found between  $AIE_r$  and  $LWC$  at Mt.  
15 Tai (Fig. 4(a)). It might due to the high aerosol loading during cloud processes (Zhao et al., 2012).

16 Although all positive  $AIE_r$  and  $AIE_N$  were found in CP-1 and CP-2, the specific values were different. According to the  
17 studies of  $AIE_r$  and  $AIE_N$  of CP-1 and CP-2, it was indicated that cloud droplets numbers are more sensitive to  $N_p$  under smaller  
18 aerosol amount conditions. The calculation of  $AIE_r$  was shown in Fig. S9 and summarized in Fig. 4. As shown in Fig. 4(a),  
19 except for the out-of-bound  $AIE_r$  values calculated with insufficient data points when  $LWC$  was larger than  $0.7 \text{ g m}^{-3}$ ,  $AIE_r$  of  
20  $0.181\text{--}0.269$  for CP-1 were always higher than those of  $0.025\text{--}0.123$  for CP-2 in corresponding narrow  $LWC$  ranges. We  
21 verified this with  $AIE_N$ . Due to the limitation of the Fog Monitor, the number of cloud droplets may be underestimated during  
22 the activation and dissipation stages (Mazoyer et al., 2019), which caused the low  $R^2$  of CP-1. In CP-2, only the data of S2 and  
23 S3 were employed to calculate  $AIE_N$  for excluding the points in S1 and S4, which may be underestimation. As shown in Fig.  
24 4(b) and Fig. 4(c) both the slope (0.144) and  $R^2$  (0.050) of CP-2 are lower than those (0.544 and 0.282, respectively) of CP-1.  
25 It verified that cloud droplets in CP-2 were little influenced by aerosols. In the previous studies, both observation and modelling  
26 studies also found that  $AIE_r$  was higher under smaller aerosol amount conditions. Twohy et al. (2005) measured the equivalent  
27  $AIE_r$  of 0.27 in the California coast while Zhao et al. (2018) used satellite observations to attribute lower values of 0.10-0.19  
28 for convective clouds over Hebei, one polluted region in China. Using an adiabatic cloud parcel model, Feingold (2003) found  
29 that  $AIE_r$  increased from 0.199 to 0.301 when  $N_p$  decreased to less than  $1000 \text{ \# cm}^{-3}$ . By using the Community Atmospheric  
30 Model version 5 (CAM5), Zhao et al. (2012) also found high  $AIE_r$  values in the tropical West Pacific at Darwin (TWP) due to  
31 the low  $N_p$  in December, January, and February. Through studying the impact of ship-produced aerosols on the microstructure

and albedo of warm marine stratocumulus clouds, Durkee et al. (2000) found that the clean and shallow boundary layers would be more readily perturbed by the addition of ship particle effluents. In the present study, the higher values of  $AIE_r$  and  $AIE_N$  of CP-1 indicated that if the same amount of aerosol particles entered the cloud, the microphysical parameters would be influenced more in CP-1 than in CP-2.

In addition, the meteorological conditions and the topography during the monitoring period would also affect the microphysical properties of clouds. During the observation period,  $CBH$  ranged from 460.3 m to 3639.1 m with the average value of 1382.5 m. The observation station would be totally enveloped in clouds and around when cloud events occurred, and the corresponding distance between the observation point and  $CBH$  was represented in Fig. 2(b). The sensitivity analysis of  $N_C$  to  $CBH$  and  $v_{up}$  was estimated by applying the equation as  $S(X_i) = \partial \ln N_C / \partial \ln X_i$ , where  $X_i$  represented  $CBH$  and  $v_{up}$ . As shown in Talbe S2, CP-2 was more sensitive to the variation of meteorological parameters if compared with CP-1. It was consistent with the study of McFiggans et al. (2006). They found that the sensitivity of  $N_C$  to  $v_{up}$  increased while the sensitivity of  $N_C$  to  $N_P$  decreased when  $N_P > 1000 \text{ \# cm}^{-3}$ . The higher values of  $S(CBH)$  and  $S(v_{up})$  of CP-2 indicated that CP-2 was more sensitive to the change of  $CBH$  and  $v_{up}$ . It might cause the periodical variations of cloud microphysical properties during CP-2.

### 3.2.3. Size distribution of cloud droplets and particles

To illustrate the evolution of the aerosol particles and the cloud droplets during the cloud processes, the size distributions of  $N_P$  and  $N_C$  during different cloud stages are plotted in Fig. 5. For each of the four size bins ranged from 2 to 13  $\mu\text{m}$ , cloud number concentrations of SL1 and SL2 were lower than those of SH1 and SH2. In the size bin of 13–50  $\mu\text{m}$ , however,  $N_C$  of SL1 and SL2 were the largest (Fig. 5(b)). This size distributions of cloud droplets in SL1 and SL2 resulted in the larger  $r_{eff}$  during the two stages, which was consistent with the result shown in Fig. 3(b). During SH1 and SH2 in CP-1, the numbers of aerosol particles in all size bins increased. But the increase of aerosol particles larger than 150 nm was the smallest, indicating that aerosols larger than 150 nm were more easily activated into cloud droplets. The activation of aerosol particles with the size larger than 150 nm in the present study dramatically increased  $N_C$  of 5–10  $\mu\text{m}$  and made  $N_C$  of SH1 and SH2 in different size bins all comparable with those of CP-2 (Fig. 5(b)).

As shown in Fig. 5(c), cloud droplets with  $D_C$  ranging from 5 to 10  $\mu\text{m}$  had high  $N_C$  in each stage in CP-2 and cloud droplets with  $D_C$  ranging from 13 to 50  $\mu\text{m}$  had low  $N_C$  in each stage if compared to CP-1. It caused the lower  $r_{eff}$  in CP-2 than CP-1. During CP-2, aerosol particles with diameters larger than 150 nm quickly decreased by activation when cloud events occurred, while the number of aerosol particles in the size of 50–150 nm were slightly influenced by cloud events (the first panel of Fig. 5(a)). It was consistent with the study of Targino et al. (2007) who found aerosol size distributions of cloud residuals, which represented aerosol particles activated to cloud droplets, peaked at about 0.15  $\mu\text{m}$  at Mt. Åreskutan. Mertes et al. (2005) also found that particles centered at  $d_p = 200 \text{ nm}$  could be efficiently activated to droplets while most Aitken mode

1 particles remained in the interstitial phase. Compared with other stages, S1 had the highest  $N_C$  in three size bins of  $[2, 5) \mu\text{m}$   
2 and  $[5, 7) \mu\text{m}$ . It indicated that large numbers of cloud droplets with small sizes were formed in the beginning of cloud events  
3 in CP-2.

### 4 **3.3. Relations among $LWC$ , $r_{eff}$ and $N_C$**

5 The 5 min averaged  $LWC$  for CP-1 and CP-2 is plotted against corresponding  $r_{eff}$  in Fig. 6(a). Large cloud droplets ( $r_{eff} > 8 \mu\text{m}$ )  
6 were observed in CP-1, while the  $r_{eff}$  for CP-2 varied narrowly in the range of  $2.5\text{--}8 \mu\text{m}$ .

7 Cloud droplets with  $r_{eff} > 8 \mu\text{m}$  only occurred in the two relatively clean stages, SL1 and SL2, during CP-1. It was due to  
8 the weaker competition among droplets at lower  $N_{CCN}$  conditions. This has also been observed in the U.S. Mid-Atlantic region  
9 where cloud droplets with larger sizes are more easily formed with lower  $N_{CCN}$  (Li et al., 2017b). At the same  $LWC$  level, the  
10 growth of cloud droplets during SH1 and SH2 was obviously limited if compared with SL1 and SL2, which is referred to as  
11 the “Twomey effect” (Twomey, 1977). This is consistent with the illustration in Fig. 3 that cloud droplets in SH1 and SH2  
12 were smaller.

13 The variation  $r_{eff}$  and/or  $N_C$  can influence  $LWC$ , while the key factor may be different in different stages of the cloud. As  
14 shown in the lower panel of Fig. 6(a), CE-20 was taken as an example to discuss the relation among  $LWC$ ,  $r_{eff}$  and  $N_C$  in  
15 different cloud stages. During S1, the existing numerous CCN (Fig. 3(a)) were quickly activated to form cloud droplets. The  
16 newly formed droplets are characterized with small sizes but large numbers. They will suppress the beginning of collision-  
17 coalescence processes (Rosenfeld et al., 2014a) and may further significantly delay raindrop formation Qian et al. (2009). In  
18 S1,  $N_C$  and  $r_{eff}$  **consistently varied**. Both the increase in  $N_C$  (from  $1188 \text{ \# cm}^{-3}$  to  $2940 \text{ \# cm}^{-3}$ ) and the growth of  $r_{eff}$  (from  $\sim 3.5$   
19  $\mu\text{m}$  to  $\sim 4.5 \mu\text{m}$ ) boosted the  $LWC$  in this stage. This is different from Mazoyer et al. (2019)’s result that they found a clearly  
20 inverse relationship between the number and the size of droplets at the beginning of the first hour of fog events during the  
21 observation in suburban Paris. When compared with fog, cloud is usually formed under conditions with more condensible  
22 water vapour (Fig. 1). The limited growth of droplets in fog will not occur in cloud. It caused the positive relationship with  
23 cloud droplet number and droplet size. At the beginning of S2,  $N_C$  reaches the maximum. The high  $N_C$  yields a great coalescence  
24 rate between cloud droplets. Meanwhile, the coalescence process is self-accelerating (Freud and Rosenfeld, 2012) and thus  
25 causes the quick decrease of  $N_C$  (Fig. 3(a)). This makes cloud droplets in S2 characterized by larger sizes as well as lower  
26 number concentrations, whilst  $LWC$  simply varies in a relatively narrow range (Fig. 6(a)). During S3,  $N_C$  is almost constant  
27 due to the formation, coagulation, and evaporation of the cloud droplets reaching a balance. As shown in the panel, the  
28 relationship between  $r_{eff}$  and  $LWC$  in this stage could be fitting as  $r_{eff} = a \times LWC^{0.34 \pm 0.02}$ , which means under the increase of  $LWC$ ,  
29 the  $N_C$  was almost unchanged. The variation of  $LWC$  values is mainly due to the changes of droplet sizes. At the dissipation  
30 stage of S4, the increase of  $CBH$  brought air with low  $RH$  and high  $N_p$  to the summit of Mt. Tai and caused the dissipation of  
31 cloud events (Fig. 2(c) and Fig. 3(a)). The previously activated CCN returned back to the interstitial aerosol phase due to the

1 evaporation of the droplets (Verheggen et al., 2007). Both  $N_C$  and  $r_{eff}$  decline. It also illustrates in Fig. 5(c) that all the  $N_C$  of  
2 the five size bins of cloud droplets decrease in S4.

3 In order to investigate the variation of  $r_{eff}$  upon  $N_C$ , the distribution of  $r_{eff}$  was classified with different  $N_C$  ranges in Fig.  
4 6(b). For  $N_C < 1000 \text{ \# cm}^{-3}$ ,  $r_{eff}$  displayed a trimodal distribution and concentrated on  $3.25 \text{ \mu m}$  (Peak-1),  $4.86 \text{ \mu m}$  (Peak-2) and  
5  $7.52 \text{ \mu m}$  (Peak-3), respectively. Peak-1 corresponded to cloud droplets with low  $N_C$ ,  $LWC$ , and  $r_{eff}$  values while the  $N_{CCN0.2}$  was  
6 very high (Fig. 6(c)). These points represented cloud droplets in the incipient stage or the dissipation stage of cloud events  
7 where large numbers of CCN exist in the atmosphere. Peak-2 and Peak-3 represented the mature stages for cloud events with  
8 different environmental conditions. Peak-3 represented cloud droplets formed under a relatively cleaner atmosphere. In this  
9 circumstance, CCN were efficiently activated and had a lower concentration remaining in the atmosphere (Fig. 6(c)). The  
10 sufficient ambient water vapour accelerated the growth of the formed droplets, which were characterized with low  $N_C$  and  
11  $LWC$  but large  $r_{eff}$ . Peak-2 represented cloud droplets formed under relatively polluted conditions and was the only peak found  
12 for  $N_C$  larger than  $1000 \text{ \# cm}^{-3}$ . With the increase of  $N_C$ , the distribution of this peak narrowed and slightly moved to lower  $r_{eff}$   
13 mode.

14 The thickness of orographic cloud was easily influenced by the specific topography and environmental conditions (Barros  
15 and Lettenmaier, 1994; Welch et al., 2008). If assuming the cloud thickness during CP-1 and CP-2 were equal, albedo would  
16 depend on the values of  $LWC$  and  $N_C$  as described in Section 2.8. Cloud albedo during CP-2 was always higher than that during  
17 CP-1, especially when the cloud thickness was lower than about 2500 m (Fig. 6(d)). **Note that the increase of  $N_C$  could enhance**  
18 **the evaporation and further reduce the lifetime of cloud, which was not taken into account when calculating the induced albedo.**  
19 Through studying marine stratocumulus clouds in the north-eastern Pacific Ocean, Twohy et al. (2005) also found that the  
20 increase of  $N_C$  by a factor of 2.8 would lead to 40% increase of albedo going from 0.325 to 0.458. It indicated that the higher  
21  $N_C$  would increase the cloud albedo if assuming no change of cloud thickness **and regardless the cloud lifetime.**

#### 22 4. Conclusion

23 From 17<sup>th</sup> June to 30<sup>th</sup> July 2018 in-situ observations of number concentrations and size distributions of aerosol particles  
24 and cloud droplets are employed to show aerosol-cloud interactions at the summit of Mt. Tai. Large variations of the  
25 characteristic values in terms of  $N_C$ ,  $LWC$  and  $r_{eff}$  were found during the observation period. Cloud droplets with smaller  $r_{eff}$   
26 and lower  $LWC$  are observed at Mt. Tai, which are similar to urban fogs.

27 Two typical cloud processes, CP-1 and CP-2, are applied to study the cloud-aerosol interactions based on the aerosol  
28 characteristics (especially  $N_P$  and  $N_{CCN}$ ) before cloud onsets. For the CP-1, which corresponded to relatively clean conditions,  
29 water content is sufficient while  **$N_{CCN}$  was considered as the limitation of cloud droplet formation according to the observation**  
30 **results.** The newly formed cloud droplets are characterized with low  $N_C$  but high  $LWC/N_C$  and large  $r_{eff}$ . With the increase of

1 aerosol concentration,  $N_C$  was found dramatically increased with a factor of three. Large numbers of  $N_{CCN}$  would compete for  
2 the system water content with the formed cloud droplets and, as a result, further dramatically decrease the  $LWC/N_C$  and  $r_{eff}$   
3 values of cloud droplets. In CP-2,  $N_P$  before the cloud onset is high and  $N_{CCN}$  is sufficient. Water vapour was considered as the  
4 limitation for cloud formation. Large numbers of small cloud droplets with low  $LWC/N_C$  were observed in the incipient stage  
5 of cloud events. In addition, periodically changes of cloud microphysical properties were found. Both consistent variation and  
6 inverse variation between  $N_P$  and  $N_C$  have been observed in the present study, which were characterized with relatively high  
7 and low  $LWC/N_C$  values, respectively.

8 Both positive  $AIE_r$  and  $AIE_N$  values observed at Mt. Tai indicate that the increase of  $N_P$  will decrease  $r_{eff}$  and increase  $N_C$   
9 of cloud droplets.  $AIE_r$  and  $AIE_N$  values are lower with higher  $N_P$  and  $N_{CCN}$ . This represents that the increase of  $N_P$  will more  
10 strongly decrease the size and increase the number of cloud droplets under the conditions of smaller aerosol amount. Through  
11 studying the size distributions of aerosol particles and cloud droplets, higher  $N_C$  in the size bin of 13–50  $\mu\text{m}$  resulted in the  
12 larger  $r_{eff}$  during the two clean stages in CP-1. Particles larger than 150 nm were possible to be efficiently activated to cloud  
13 droplets and make important contributions to the increase of cloud droplets in the size range of 5–10  $\mu\text{m}$ .

14 The  $LWC$  of cloud depended on the change of  $r_{eff}$  and  $N_C$ . However, the decisive factor may differ at different stages of  
15 the cloud. In general, the  $r_{eff}$  of cloud droplets consistently varied with  $LWC$ . But in different  $N_C$  ranges, the  $r_{eff}$  of cloud droplets  
16 were observed with different distribution shapes. For  $N_C < 1000 \text{ \# cm}^{-3}$ ,  $r_{eff}$  displayed a trimodal distribution. Three peaks were  
17 3.25, 4.86 and 7.52  $\mu\text{m}$ , respectively. With the increase of  $N_C$ , a narrowed unimodal distribution of  $r_{eff}$  appeared and the peak  
18 value slightly moved towards lower  $r_{eff}$  mode. For a constant cloud thickness and regardless the cloud lifetime, the increased  
19  $N_C$  and decreased  $r_{eff}$  dramatically increase the cloud albedo, which may further influence the regional climate in the North  
20 China Plain.

21 The local topography of the surrounding areas at Mt. Tai supplies a potential access for aerosol transportation and can  
22 affect the measured cloud droplet distributions by increasing turbulence or causing orographic flows. Even though the summit  
23 of Mt. Tai is far away from the polluted sources, the transported CCN could change the cloud microphysical properties (i.e.,  
24 during CP-1). The cloud microphysical parameters derived in our study characterized the cloud features in the North China  
25 Plain, and provided valuable data for modelling studies of cloud microphysics in the future.

## 26 Data availability

27 All data used to support the conclusion are presented in this paper. Additional data are available upon request. Please  
28 contact the corresponding authors Jianmin Chen (jmchen@fudan.edu.cn) and Hui Chen ([hui\\_chen@fudan.edu.cn](mailto:hui_chen@fudan.edu.cn)).

## 29 Author contribution.

30 JC, HC conceived the study. JL and CZ performed the field experiments and sampled cloud water. JL analysed the data

1 and wrote the main manuscript text. JC, HC, DZ, CZ and HH revised the initial manuscript. LX, XW and HL supported  
2 the meteorological data and PM<sub>2.5</sub> mass concentration. PL, JL, CZ, YM and WZ assisted in instrument maintenance. LZ,  
3 KL and ML contributed to the organization and arrangement of the field observation. LZ provided the meteorological  
4 parameters of Tai'an City. All of the authors discussed the results, and contributed to the final manuscript.

#### 5 **Competing interests.**

6 The authors declare no conflict of interest.

#### 7 **Acknowledgement**

8 This work was supported by the Ministry of Science and Technology of China (2016YFC0202700), Tai'an Research  
9 Project (SDTASJ2018-0761-00), National Natural Science Foundation of China (91843301, 91743202, 41805091,  
10 21806020), and Marie Skłodowska-Curie Actions (690958-MARSU-RISE-2015).  
11



## 1 References

- 2 Albrecht, B. A.: Aerosols, cloud microphysics, and fractional cloudiness, *Science*, 245, 1227-1230,  
3 10.1126/science.245.4923.1227, 1989.
- 4 Allan, J. D., Baumgardner, D., Raga, G. B., Mayol-Bracero, O. L., Morales-Garcia, F., Garcia-Garcia, F., Montero-Martinez,  
5 G., Borrmann, S., Schneider, J., Mertes, S., Walter, S., Gysel, M., Dusek, U., Frank, G. P., and Kraemer, M.: Clouds and  
6 aerosols in Puerto Rico - a new evaluation, *Atmos. Chem. Phys.*, 8, 1293-1309, 10.5194/acp-8-1293-2008, 2008.
- 7 Andreae, M. O., Rosenfeld, D., Artaxo, P., Costa, A. A., Frank, G. P., Longo, K. M., and Silva-Dias, M. A. F.: Smoking rain  
8 clouds over the Amazon, *Science*, 303, 1337-1342, 10.1126/science.1092779, 2004.
- 9 Barros, A. P., and Lettenmaier, D. P.: DYNAMIC MODELING OF OROGRAPHICALLY INDUCED PRECIPITATION,  
10 *Reviews of Geophysics*, 32, 265-284, 10.1029/94rg00625, 1994.
- 11 Boutle, I., Price, J., Kudzsotsa, I., Kokkola, H., and Romakkaniemi, S.: Aerosol-fog interaction and the transition to well-mixed  
12 radiation fog, *Atmos. Chem. Phys.*, 18, 7827-7840, 10.5194/acp-18-7827-2018, 2018.
- 13 Chang, Y., Zhang, Y., Li, J., Tian, C., Song, L., Zhai, X., Zhang, W., Huang, T., Lin, Y. C., Zhu, C., Fang, Y., Lehmann, M. F.,  
14 and Chen, J.: Isotopic Constraints on the Atmospheric Sources and Formation of Nitrogenous Species in Biomass-  
15 Burning-Influenced Clouds, *Atmos. Chem. Phys. Discuss.*, 2018, 1-27, 10.5194/acp-2018-1196, 2018.
- 16 Chang, Y., Guo, X., Tang, J., and Lu, G.: Aircraft measurement campaign on summer cloud microphysical properties over the  
17 Tibetan Plateau, *Sci. Rep.*, 9, 10.1038/s41598-019-41514-5, 2019.
- 18 Choularton, T. W., Colville, R. N., Bower, K. N., Gallagher, M. W., Wells, M., Beswick, K. M., Arends, B. G., Mols, J. J., Kos,  
19 G. P. A., Fuzzi, S., Lind, J. A., Orsi, G., Facchini, M. C., Laj, P., Gieray, R., Wieser, P., Engelhardt, T., Berner, A., Kruisz,  
20 C., Moller, D., Acker, K., Wieprecht, W., Luttke, J., Levsen, K., Bizjak, M., Hansson, H. C., Cederfelt, S. I., Frank, G.,  
21 Montes, B., Martinsson, B., Orsini, D., Svenningsson, B., Swietlicki, E., Wiedensohler, A., Noone, K. J., Pahl, S., Winkler,  
22 P., Seyffer, E., Helas, G., Jaeschke, W., Georgii, H. W., Wobrock, W., Preiss, M., Maser, R., Schell, D., Dollard, G., Jones,  
23 B., Davies, T., Sedlak, D. L., David, M. M., Wendisch, M., Cape, J. N., Hargreaves, K. J., Sutton, M. A., StoretonWest,  
24 R. L., Fowler, D., Hallberg, A., Harrison, R. M., and Peak, J. D.: The Great Dun Fell Cloud Experiment 1993: An overview,  
25 *Atmospheric Environment*, 31, 2393-2405, 10.1016/s1352-2310(96)00316-0, 1997.
- 26 Croft, B., Lohmann, U., Martin, R. V., Stier, P., Wurzler, S., Feichter, J., Hoose, C., Heikkila, U., van Donkelaar, A., and  
27 Ferrachat, S.: Influences of in-cloud aerosol scavenging parameterizations on aerosol concentrations and wet deposition  
28 in ECHAM5-HAM, *Atmos. Chem. Phys.*, 10, 1511-1543, 10.5194/acp-10-1511-2010, 2010.
- 29 Cross, E. S., Slowik, J. G., Davidovits, P., Allan, J. D., Worsnop, D. R., Jayne, J. T., Lewis †, D. K., Canagaratna, M., and  
30 Onasch, T. B.: Laboratory and Ambient Particle Density Determinations using Light Scattering in Conjunction with  
31 Aerosol Mass Spectrometry, *Aerosol Sci. Technol.*, 41, 343-359, 10.1080/02786820701199736, 2007.
- 32 Demoz, B. B., Collett, J. L., and Daube, B. C.: On the Caltech Active Strand Cloudwater Collectors, *Atmos. Res.*, 41, 47-62,  
33 10.1016/0169-8095(95)00044-5, 1996.
- 34 Deng, Z., Zhao, C., Zhang, Q., Huang, M., and Ma, X.: Statistical analysis of microphysical properties and the parameterization  
35 of effective radius of warm clouds in Beijing area, *Atmos. Res.*, 93, 888-896, 2009.
- 36 Drewnick, F., Schneider, J., Hings, S. S., Hock, N., Noone, K., Targino, A., Weimer, S., and Borrmann, S.: Measurement of  
37 ambient, interstitial, and residual aerosol particles on a mountaintop site in central Sweden using an aerosol mass  
38 spectrometer and a CVI, *Journal of Atmospheric Chemistry*, 56, 1-20, 10.1007/s10874-006-9036-8, 2007.
- 39 Durkee, P. A., Noone, K. J., Ferek, R. J., Johnson, D. W., Taylor, J. P., Garrett, T. J., Hobbs, P. V., Hudson, J. G., Bretherton,  
40 C. S., Innis, G., Frick, G. M., Hoppel, W. A., O'Dowd, C. D., Russell, L. M., Gasparovic, R., Nielsen, K. E., Tessmer, S.  
41 A., Ostrom, E., Osborne, S. R., Flagan, R. C., Seinfeld, J. H., and Rand, H.: The impact of ship-produced aerosols on the  
42 microstructure and albedo of warm marine stratocumulus clouds: A test of MAST hypotheses 1i and 1ii, *Journal of the*  
43 *Atmospheric Sciences*, 57, 2554-2569, 10.1175/1520-0469(2000)057<2554:Tiospa>2.0.Co;2, 2000.
- 44 Dusek, U., Frank, G. P., Hildebrandt, L., Curtius, J., Schneider, J., Walter, S., Chand, D., Drewnick, F., Hings, S., Jung, D.,  
45 Borrmann, S., and Andreae, M. O.: Size matters more than chemistry for cloud-nucleating ability of aerosol particles,  
46 *Science*, 312, 1375-1378, 10.1126/science.1125261, 2006.

1 Ekman, A. M. L., Engstrom, A., and Soderberg, A.: Impact of Two-Way Aerosol-Cloud Interaction and Changes in Aerosol  
2 Size Distribution on Simulated Aerosol-Induced Deep Convective Cloud Sensitivity, *J. Atmos. Sci.*, 68, 685-698,  
3 10.1175/2010jas3651.1, 2011.

4 Fan, J., Leung, L. R., Rosenfeld, D., Chen, Q., Li, Z., Zhang, J., and Yan, H.: Microphysical effects determine macrophysical  
5 response for aerosol impacts on deep convective clouds, *Proc. Natl. Acad. Sci. U. S. A.*, 110, E4581-E4590,  
6 10.1073/pnas.1316830110, 2013.

7 Fan, J., Wang, Y., Rosenfeld, D., and Liu, X.: Review of Aerosol-Cloud Interactions: Mechanisms, Significance, and  
8 Challenges, *J. Atmos. Sci.*, 73, 4221-4252, 10.1175/jas-d-16-0037.1, 2016.

9 Feingold, G., Remer, L. A., Ramaprasad, J., and Kaufman, Y. J.: Analysis of smoke impact on clouds in Brazilian biomass  
10 burning regions: An extension of Twomey's approach, *J. Geophys. Res.: Atmos.*, 106, 22907-22922,  
11 10.1029/2001jd000732, 2001.

12 Feingold, G.: Modeling of the first indirect effect: Analysis of measurement requirements, *Geophys. Res. Lett.*, 30,  
13 10.1029/2003gl017967, 2003.

14 Freud, E., and Rosenfeld, D.: Linear relation between convective cloud drop number concentration and depth for rain initiation,  
15 *J. Geophys. Res.: Atmos.*, 117, 13, 10.1029/2011jd016457, 2012.

16 Frey, L., Bender, F. A. M., and Svensson, G.: Cloud albedo changes in response to anthropogenic sulfate and non-sulfate  
17 aerosol forcings in CMIP5 models, *Atmos. Chem. Phys.*, 17, 9145-9162, 10.5194/acp-17-9145-2017, 2017.

18 Georgakakos, K. P., and Bras, R. L.: A hydrologically useful station precipitation model. I. Formulation, *Water Resources*  
19 *Research*, 20, 1585-1596, 10.1029/WR020i011p01585, 1984.

20 Grabowski, W. W., and Wang, L.-P.: Growth of Cloud Droplets in a Turbulent Environment, *Annu. Rev. Fluid Mech.*, 45, 293-  
21 324, 10.1146/annurev-fluid-011212-140750, 2013.

22 Guo, J., Wang, Y., Shen, X. H., Wang, Z., Lee, T., Wang, X. F., Li, P. H., Sun, M. H., Collett, J. L., Wang, W. X., and Wang,  
23 T.: Characterization of cloud water chemistry at Mount Tai, China: Seasonal variation, anthropogenic impact, and cloud  
24 processing, *Atmospheric Environment*, 60, 467-476, 10.1016/j.atmosenv.2012.07.016, 2012.

25 Heikenfeld, M., White, B., Labbouz, L., and Stier, P.: Aerosol effects on deep convection: the propagation of aerosol  
26 perturbations through convective cloud microphysics, *Atmos. Chem. Phys.*, 19, 2601-2627, 10.5194/acp-19-2601-2019,  
27 2019.

28 Heintzenberg, J., Ogren, J. A., Noone, K. J., and Gardneus, L.: The Size Distribution of Submicrometer Particles within and  
29 about Stratocumulus Cloud Droplets on Mt. Areskutan, Sweden, *Atmospheric Research*, 24, 89-101, 10.1016/0169-  
30 8095(89)90039-2, 1989.

31 Hudson, J. G.: Variability of the relationship between particle size and cloud-nucleating ability, *Geophys. Res. Lett.*, 34,  
32 10.1029/2006gl028850, 2007.

33 Khain, A. P., Beheng, K. D., Heymsfield, A., Korolev, A., Krichak, S. O., Levin, Z., Pinsky, M., Phillips, V., Prabhakaran, T.,  
34 Teller, A., van den Heever, S. C., and Yano, J. I.: Representation of microphysical processes in cloud-resolving models:  
35 Spectral (bin) microphysics versus bulk parameterization, *Rev. Geophys.*, 53, 247-322, 10.1002/2014rg000468, 2015.

36 Koren, I., Kaufman, Y. J., Rosenfeld, D., Remer, L. A., and Rudich, Y.: Aerosol invigoration and restructuring of Atlantic  
37 convective clouds, *Geophys. Res. Lett.*, 32, 10.1029/2005gl023187, 2005.

38 Lacis, A. A., and Hansen, J. E.: Parameterization for absorption of solar-radiation in earths atmosphere *J. Atmos. Sci.*, 31, 118-  
39 133, 10.1175/1520-0469(1974)031<0118:Apftao>2.0.Co;2, 1974.

40 Li, J., Wang, X., Chen, J., Chao, Z., and Herrmann, H.: Chemical composition and droplet size distribution of cloud at the  
41 summit of Mount Tai, China, *Atmos. Chem. Phys.*, 17, 1-21, 2017a.

42 Li, P., Li, X., Yang, C., Wang, X., Chen, J., and Jr, J. L. C.: Fog water chemistry in Shanghai, *Atmos. Environ.*, 45, 4034-4041,  
43 2011.

44 Li, S., Joseph, E., Min, Q., and Yin, B.: Multi-year ground-based observations of aerosol-cloud interactions in the Mid-Atlantic  
45 of the United States, *J. Quant. Spectrosc. Radiat. Transfer*, 188, 192-199, 10.1016/j.jqsrt.2016.02.004, 2017b.

46 Lohmann, U., and Feichter, J.: Global indirect aerosol effects: a review, *Atmos. Chem. Phys.*, 5, 715-737, 10.5194/acp-5-715-  
47 2005, 2005.

1 Lu, C., Niu, S., Tang, L., Lv, J., Zhao, L., and Zhu, B.: Chemical composition of fog water in Nanjing area of China and its  
2 related fog microphysics, *Atmos. Res.*, 97, 47-69, 2010.

3 Lu, M.-L., Conant, W. C., Jonsson, H. H., Varutbangkul, V., Flagan, R. C., and Seinfeld, J. H.: The Marine  
4 Stratus/Stratocumulus Experiment (MASE): Aerosol-cloud relationships in marine stratocumulus, *J. Geophys. Res.:*  
5 *Atmos.*, 112, 10.1029/2006jd007985, 2007.

6 Mazoyer, M., Burnet, F., Denjean, C., Roberts, G. C., Haeffelin, M., Dupont, J. C., and Elias, T.: Experimental study of the  
7 aerosol impact on fog microphysics, *Atmos. Chem. Phys.*, 19, 4323-4344, 10.5194/acp-19-4323-2019, 2019.

8 McComiskey, A., Feingold, G., Frisch, A. S., Turner, D. D., Miller, M. A., Chiu, J. C., Min, Q., and Ogren, J. A.: An assessment  
9 of aerosol-cloud interactions in marine stratus clouds based on surface remote sensing, *J. Geophys. Res.: Atmos.*, 114, -,  
10 2009.

11 McFiggans, G., Artaxo, P., Baltensperger, U., Coe, H., Facchini, M. C., Feingold, G., Fuzzi, S., Gysel, M., Laaksonen, A.,  
12 Lohmann, U., Mentel, T. F., Murphy, D. M., O'Dowd, C. D., Snider, J. R., and Weingartner, E.: The effect of physical and  
13 chemical aerosol properties on warm cloud droplet activation, *Atmos. Chem. Phys.*, 6, 2593-2649, 10.5194/acp-6-2593-  
14 2006, 2006.

15 Mertes, S., Galgon, D., Schwirn, K., Nowak, A., Lehmann, K., Massling, A., Wiedensohler, A., and Wieprecht, W.: Evolution  
16 of particle concentration and size distribution observed upwind, inside and downwind hill cap clouds at connected flow  
17 conditions during FEBUKO, *Atmos. Environ.*, 39, 4233-4245, 10.1016/j.atmosenv.2005.02.009, 2005.

18 Modini, R. L., Frossard, A. A., Ahlm, L., Russell, L. M., Corrigan, C. E., Roberts, G. C., Hawkins, L. N., Schroder, J. C.,  
19 Bertram, A. K., Zhao, R., Lee, A. K. Y., Abbatt, J. P. D., Lin, J., Nenes, A., Wang, Z., Wonaschuetz, A., Sorooshian, A.,  
20 Noone, K. J., Jonsson, H., Seinfeld, J. H., Toom-Sauntry, D., Macdonald, A. M., and Leaitch, W. R.: Primary marine  
21 aerosol-cloud interactions off the coast of California, *Journal of Geophysical Research-Atmospheres*, 120, 4282-4303,  
22 10.1002/2014jd022963, 2015.

23 Möller, D., Acker, K., and Wieprecht, W.: A relationship between liquid water content and chemical composition in clouds,  
24 *Atmos. Res.*, 41, 321-335, 1996.

25 Noone, K. J., Ogren, J. A., and Heintzenberg, J.: An Examination of Clouds at a Mountain-Top Site in Central Sweden: The  
26 Distribution of Solute within Cloud Droplets, *Atmospheric Research*, 25, 3-15, 10.1016/0169-8095(90)90002-t, 1990.

27 Padmakumari, B., Mahes Kumar, R. S., Anand, V., and Axisa, D.: Microphysical characteristics of convective clouds over ocean  
28 and land from aircraft observations, *Atmos. Res.*, 195, 62-71, 10.1016/j.atmosres.2017.05.011, 2017.

29 Penner, J. E., Dong, X. Q., and Chen, Y.: Observational evidence of a change in radiative forcing due to the indirect aerosol  
30 effect, *Nature*, 427, 231-234, 10.1038/nature02234, 2004.

31 Qian, Y., Gong, D. Y., Fan, J. W., Leung, L. R., Bennartz, R., Chen, D. L., and Wang, W. G.: Heavy pollution suppresses light  
32 rain in China: Observations and modeling, *J. Geophys. Res.: Atmos.*, 114, 16, 10.1029/2008jd011575, 2009.

33 Quante, M.: The role of clouds in the climate system, *J. Phys. IV*, 121, 61-86, 10.1051/jp4:2004121003, 2004.

34 Reid, J. S., Hobbs, P. V., Rangno, A. L., and Hegg, D. A.: Relationships between cloud droplet effective radius, liquid water  
35 content, and droplet concentration for warm clouds in Brazil embedded in biomass smoke, *J. Geophys. Res.: Atmos.*, 104,  
36 6145-6153, 1999.

37 Rose, D., Gunthe, S. S., Mikhailov, E., Frank, G. P., Dusek, U., Andreae, M. O., and Poeschl, U.: Calibration and measurement  
38 uncertainties of a continuous-flow cloud condensation nuclei counter (DMT-CCNC): CCN activation of ammonium  
39 sulfate and sodium chloride aerosol particles in theory and experiment, *Atmospheric Chemistry and Physics*, 8, 1153-  
40 1179, 10.5194/acp-8-1153-2008, 2008.

41 Rosenfeld, D.: Aerosol-cloud interactions control of earth radiation and latent heat release budgets, *Space Sci. Rev.*, 125, 149-  
42 157, 10.1007/s11214-006-9053-6, 2006.

43 Rosenfeld, D., Andreae, M. O., Asmi, A., Chin, M., de Leeuw, G., Donovan, D. P., Kahn, R., Kinne, S., Kivekas, N., Kulmala,  
44 M., Lau, W., Schmidt, K. S., Suni, T., Wagner, T., Wild, M., and Quaas, J.: Global observations of aerosol-cloud-  
45 precipitation-climate interactions, *Rev. Geophys.*, 52, 750-808, 10.1002/2013rg000441, 2014a.

46 Rosenfeld, D., Sherwood, S., Wood, R., and Donner, L.: Climate Effects of Aerosol-Cloud Interactions, *Science*, 343, 379-  
47 380, 10.1126/science.1247490, 2014b.

1 Roth, A., Schneider, J., Klimach, T., Mertes, S., van Pinxteren, D., Herrmann, H., and Borrmann, S.: Aerosol properties, source  
2 identification, and cloud processing in orographic clouds measured by single particle mass spectrometry on a central  
3 European mountain site during HCCT-2010, *Atmos. Chem. Phys.*, 16, 505-524, 10.5194/acp-16-505-2016, 2016.

4 Sant, V., Lohmann, U., and Seifert, A.: Performance of a Triclass Parameterization for the Collision-Coalescence Process in  
5 Shallow Clouds, *J. Atmos. Sci.*, 70, 1744-1767, 10.1175/jas-d-12-0154.1, 2013.

6 Schroder, J. C., Hanna, S. J., Modini, R. L., Corrigan, A. L., Kreidenwies, S. M., Macdonald, A. M., Noone, K. J., Russell, L.  
7 M., Leaitch, W. R., and Bertram, A. K.: Size-resolved observations of refractory black carbon particles in cloud droplets  
8 at a marine boundary layer site, *Atmospheric Chemistry and Physics*, 15, 1367-1383, 10.5194/acp-15-1367-2015, 2015.

9 Seinfeld, J. H., and Pandis, S. N.: *Atmospheric Chemistry and Physics: From Air Pollution to Climate Change*, John Wiley &  
10 Sons, Inc., Hoboken, New Jersey, 2006.

11 Seinfeld, J. H., Bretherton, C., Carslaw, K. S., Coe, H., DeMott, P. J., Dunlea, E. J., Feingold, G., Ghan, S., Guenther, A. B.,  
12 Kahn, R., Kraucunas, I., Kreidenweis, S. M., Molina, M. J., Nenes, A., Penner, J. E., Prather, K. A., Ramanathan, V.,  
13 Ramaswamy, V., Rasch, P. J., Ravishankara, A. R., Rosenfeld, D., Stephens, G., and Wood, R.: Improving our fundamental  
14 understanding of the role of aerosol-cloud interactions in the climate system, *Proc. Natl. Acad. Sci. U. S. A.*, 113, 5781-  
15 5790, 2016.

16 Shen, L., Wang, H., Yin, Y., Chen, J., and Chen, K.: Observation of atmospheric new particle growth events at the summit of  
17 mountain Tai (1534 m) in Central East China, *Atmos. Environ.*, 201, 148-157, 10.1016/j.atmosenv.2018.12.051, 2019.

18 Spiegel, J. K., Zieger, P., Bukowiecki, N., Hammer, E., Weingartner, E., and Eugster, W.: Evaluating the capabilities and  
19 uncertainties of droplet measurements for the fog droplet spectrometer (FM-100), *Atmospheric Measurement Techniques*,  
20 5, 2237-2260, 10.5194/amt-5-2237-2012, 2012.

21 Stephens, G. L.: Radiation profiles in extended water clouds. II. Parameterization schemes, *Journal of the Atmospheric*  
22 *Sciences*, 35, 2123-2132, 10.1175/1520-0469(1978)035<2123:Rpiewc>2.0.Co;2, 1978.

23 Stevens, B., and Bony, S.: What Are Climate Models Missing?, *Science*, 340, 1053-1054, 10.1126/science.1237554, 2013.

24 Tang, J. P., Wang, P. C., Mickley, L. J., Xia, X. G., Liao, H., Yue, X., Sun, L., and Xia, J. R.: Positive relationship between  
25 liquid cloud droplet effective radius and aerosol optical depth over Eastern China from satellite data, *Atmos. Environ.*,  
26 48, 244-253, 10.1016/j.atmosenv.2013.08.024, 2014.

27 Targino, A. C., Noone, K. J., Drewnick, F., Schneider, J., Krejci, R., Olivares, G., Hings, S., and Borrmann, S.: Microphysical  
28 and chemical characteristics of cloud droplet residuals and interstitial particles in continental stratocumulus clouds,  
29 *Atmospheric Research*, 86, 225-240, 10.1016/j.atmosres.2007.05.001, 2007.

30 Twohy, C. H., Petters, M. D., Snider, J. R., Stevens, B., Tahnk, W., Wetzell, M., Russell, L., and Burnet, F.: Evaluation of the  
31 aerosol indirect effect in marine stratocumulus clouds: Droplet number, size, liquid water path, and radiative impact, *J.*  
32 *Geophys. Res.: Atmos.*, 110, -, 2005.

33 Twomey, S.: Pollution and planetary albedo, *Atmos. Environ.*, 8, 1251-1256, 10.1016/0004-6981(74)90004-3, 1974.

34 Twomey, S. A.: The Influence of Pollution on the Shortwave Albedo of Clouds, *J. Atmos. Sci.*, 34, 1149-1154, 1977.

35 Van Pinxteren, D., Fomba, K. W., Mertes, S., Müller, K., Spindler, G., Schneider, J., Lee, T., Collett, J. L., and Herrmann, H.:  
36 Cloud water composition during HCCT-2010: Scavenging efficiencies, solute concentrations, and droplet size  
37 dependence of inorganic ions and dissolved organic carbon, *Atmos. Chem. Phys.*, 15, 24311-24368, 2016.

38 Verheggen, B., Cozic, J., Weingartner, E., Bower, K., Mertes, S., Connolly, P., Gallagher, M., Flynn, M., Choulaton, T., and  
39 Baltensperger, U.: Aerosol partitioning between the interstitial and the condensed phase in mixed-phase clouds, *Journal*  
40 *of Geophysical Research-Atmospheres*, 112, 13, 10.1029/2007jd008714, 2007.

41 Wang, Y., Guo, J., Wang, T., Ding, A., Gao, J., Yang, Z., Jr, J. L. C., and Wang, W.: Influence of regional pollution and  
42 sandstorms on the chemical composition of cloud/fog at the summit of Mt. Taishan in northern China, *Atmos. Res.*, 99,  
43 434-442, 2011.

44 Welch, R. M., Asefi, S., Zeng, J., Nair, U. S., Han, Q., Lawton, R. O., Ray, D. K., and Manoharan, V. S.: Biogeography of  
45 tropical montane cloud forests. Part I: Remote sensing of cloud-base heights, *Journal of Applied Meteorology and*  
46 *Climatology*, 47, 960-975, 10.1175/2007jamc1668.1, 2008.

47 Yuan, T., Li, Z., Zhang, R., and Fan, J.: Increase of cloud droplet size with aerosol optical depth: An observation and modeling

study, *J. Geophys. Res.: Atmos.*, 113, 10.1029/2007jd008632, 2008.

Zhang, L. M., Michelangeli, D. V., and Taylor, P. A.: Numerical studies of aerosol scavenging by low-level, warm stratiform clouds and precipitation, *Atmos. Environ.*, 38, 4653-4665, 10.1016/j.atmosenv.2004.05.042, 2004a.

Zhang, X., Musson-Genon, L., Dupont, E., Milliez, M., and Carissimo, B.: On the Influence of a Simple Microphysics Parametrization on Radiation Fog Modelling: A Case Study During ParisFog, *Boundary-Layer Meteorol.*, 151, 293-315, 10.1007/s10546-013-9894-y, 2014.

Zhang, Y., Rossow, W. B., Lacis, A. A., Oinas, V., and Mishchenko, M. I.: Calculation of radiative fluxes from the surface to top of atmosphere based on ISCCP and other global data sets: Refinements of the radiative transfer model and the input data, *J. Geophys. Res.: Atmos.*, 109, 10.1029/2003JD004457 *J. Geophys. Res.* 2018/12/31 doi: 10.1029/2003JD004457, 2004b.

Zhao, C., Klein, S. A., Xie, S., Liu, X., Boyle, J. S., and Zhang, Y.: Aerosol First Indirect Effects on Non-Precipitating Low-Level Liquid Cloud Properties as Simulated by CAM5 at ARM Sites, *AGU Fall Meeting*, 2012, 376-395,

Zhao, C., Qiu, Y., Dong, X., Wang, Z., Peng, Y., Li, B., Wu, Z., and Wang, Y.: Negative Aerosol-Cloud re Relationship from Aircraft Observations over Hebei, China, *Earth Space Sci.*, 5, 2018.

Zhou, Y., Wang, T., Gao, X., Xue, L., Wang, X., Wang, Z., Gao, J., Zhang, Q., and Wang, W.: Continuous observations of water-soluble ions in PM 2.5 at Mount Tai (1534 m a.s.l.) in central-eastern China, *J. Atmos. Chem.*, 64, 107-127, 2009.

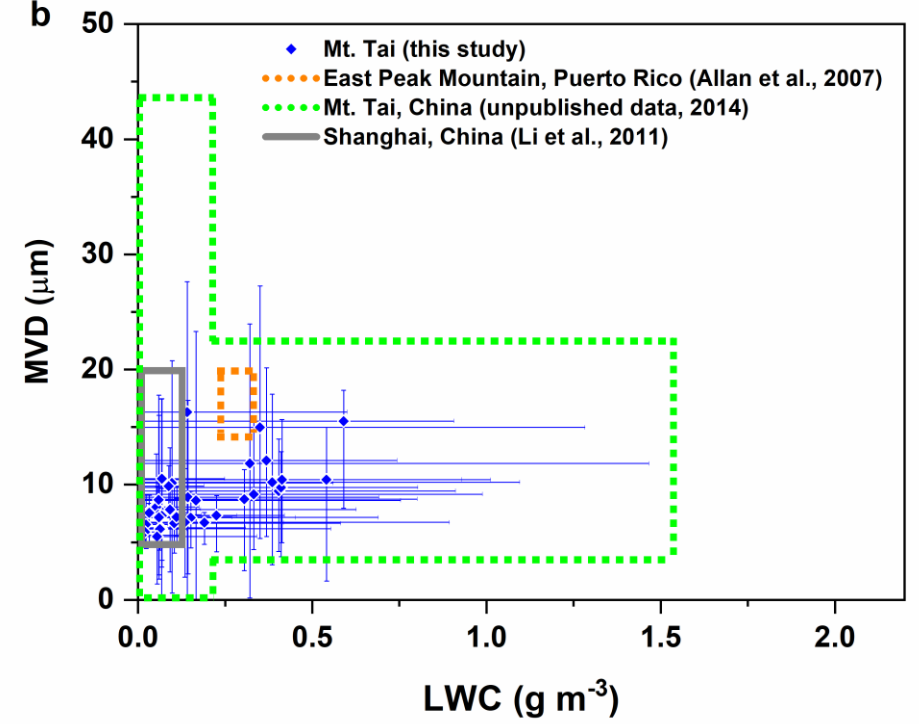
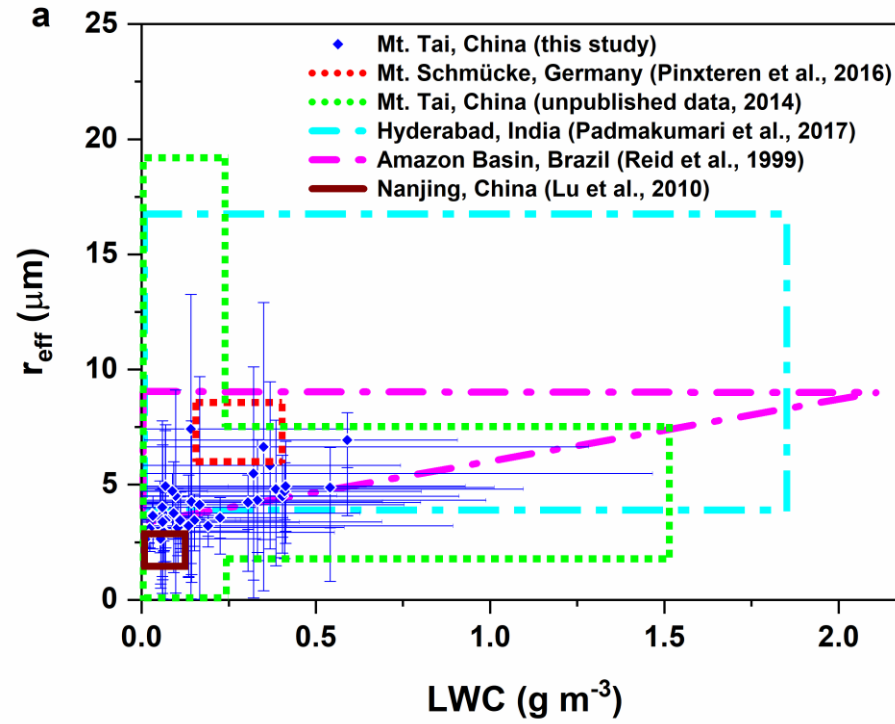
Zhu, C., Chen, J., Wang, X., Li, J., Wei, M., Xu, C., Xu, X., Ding, A., and Collett, J. L., Jr.: Chemical Composition and Bacterial Community in Size-Resolved Cloud Water at the Summit of Mt. Tai, China, *Aerosol Air Qual. Res.*, 18, 1-14, 10.4209/aaqr.2016.11.0493, 2018.

## Tables and Figures

**Table 1: Comparison of clouds monitored at Mt. Tai with city fogs, convective clouds monitored by research aircrafts and other orographic clouds. Including sampling information (site, period and altitude), the range of PM<sub>2.5</sub> mass concentrations, the range of microphysical parameters (number concentrations of cloud droplets- $N_c$ , liquid water content- $LWC$ , median volume diameter-  $MVD$ , effective radius- $r_{eff}$ ) and the number of monitored clouds/cloud events/fog events.**

Sampling Site	Period	Altitude (m a.s.l)	PM <sub>2.5</sub> ( $\mu\text{g m}^{-3}$ )	$N_c$ ( $\# \text{ cm}^{-3}$ )	$LWC$ ( $\text{g m}^{-3}$ )	$MVD$ ( $\mu\text{m}$ )	$r_{eff}$ ( $\mu\text{m}$ )	Number of clouds/cloud events/fog events	Reference
<b>City Fog</b>									
Shanghai, China	Nov. 2009	7	-	11-565	0.01-0.14	5.0-20.0	-	1	(Li et al., 2011)
Nanjing, China	Dec. 2006- Dec. 2007	22	0.03 <sup>a</sup> -0.60 <sup>a</sup>	-	2.69e <sup>-3</sup> -0.16	-	1.6 <sup>b</sup> -2.7 <sup>b</sup>	7	(Lu et al., 2010)
<b>Convective Clouds</b>									
Amazon Basin/cerrado reCompagions, Brazil	Aug.-Sept. 1995	90-4000	-	-	0 <sup>d</sup> -2.10 <sup>d</sup>	-	2.8 <sup>d</sup> -9.2 <sup>d</sup>	>1000	(Reid et al., 1999)
Hyderabad - The Bay of Bengal, India	29 <sup>th</sup> Oct. 2010	1300- 6300		10 <sup>d</sup> -380	0 <sup>d</sup> -1.80		3.8 <sup>d</sup> -17.0	1	(Padmakumari et al., 2017)
<b>Orographic clouds</b>									
Mt. Schmücke, Germany	Sep.-Oct. 2010	937	-	-	0.14-0.37	-	5.7-8.7	8	(Van Pinxteren et al., 2016)
East Peak Mountain, Puerto Rico	Dec. 2004	1040	-	193-519	0.24-0.31	14.0-20.0	-	2	(Allan et al., 2008)
Mt. Tai, China	Jul.-Aug. 2014	1545	11.1-173.3	4-2186	0.01-1.52	1.6-43.0	0.8-18.9	24	Unpublished data from (Li et al., 2017a)
Mt. Tai, China	Jun.-Jul. 2018	1545	1.2-127.1	10-3163	1.01e <sup>-3</sup> -1.47	4.4-25.0	2.4-13.4	40	This study
Mt. Tai, China (CP-1°)	10 <sup>th</sup> – 13 <sup>th</sup> Jul. 2018	1545	1.3-40.7	11-2470	1.12e <sup>-3</sup> -1.47	4.6-17.4	2.5-10.7	12	This study
Mt. Tai, China (CP-2°)	13 <sup>th</sup> – 20 <sup>th</sup> Jul. 2018	1545	1.2-66.2	10-3163	1.03e <sup>-3</sup> -1.10	4.6-13.5	2.4-7.9	12	This study

<sup>a</sup> Represents the mass concentrations of PM<sub>10</sub>. <sup>b</sup> Represents the range of averaged radius. <sup>c</sup> Two cloud processes which are detailedly discussed in this study. <sup>d</sup> Values were read from the graphs.



1  
2 **Figure 1: Plots of effective radius ( $r_{eff}$ , a) or medium volume diameter ( $MVD$ , b) against liquid water content ( $LWC$ ) for clouds and fogs from the literatures. “.....”, “- .”**  
3 **and “—” represents orographic clouds, convective clouds and city fogs, respectively. The areas represented the range of data obtained from the corresponding observations.**  
4 **The blue diamonds with error bars represented the average  $LWC$  and  $r_{eff}$  (or  $MVD$ ) of 40 cloud events observed at Mt. Tai in the present study with corresponding ranges.**



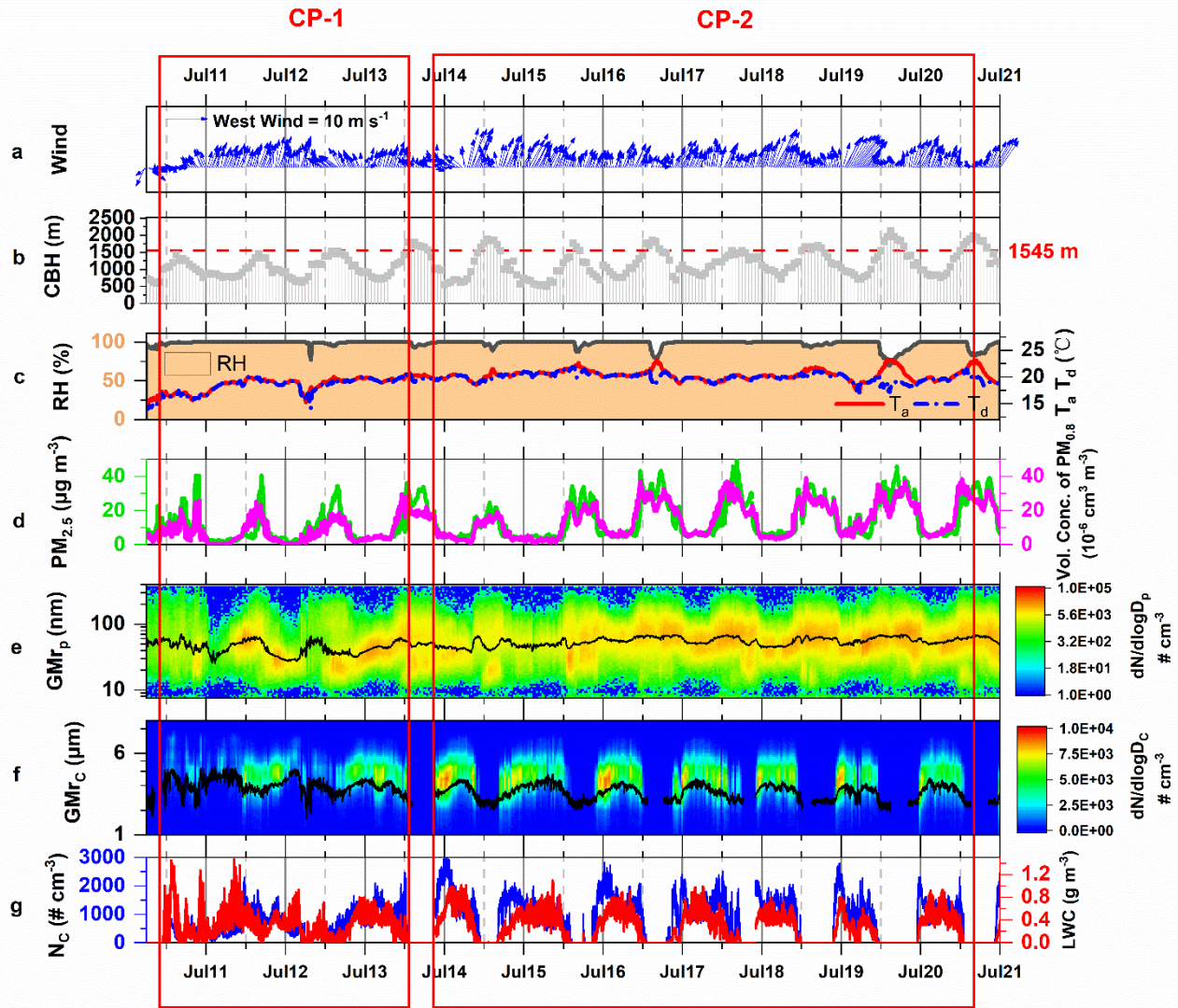
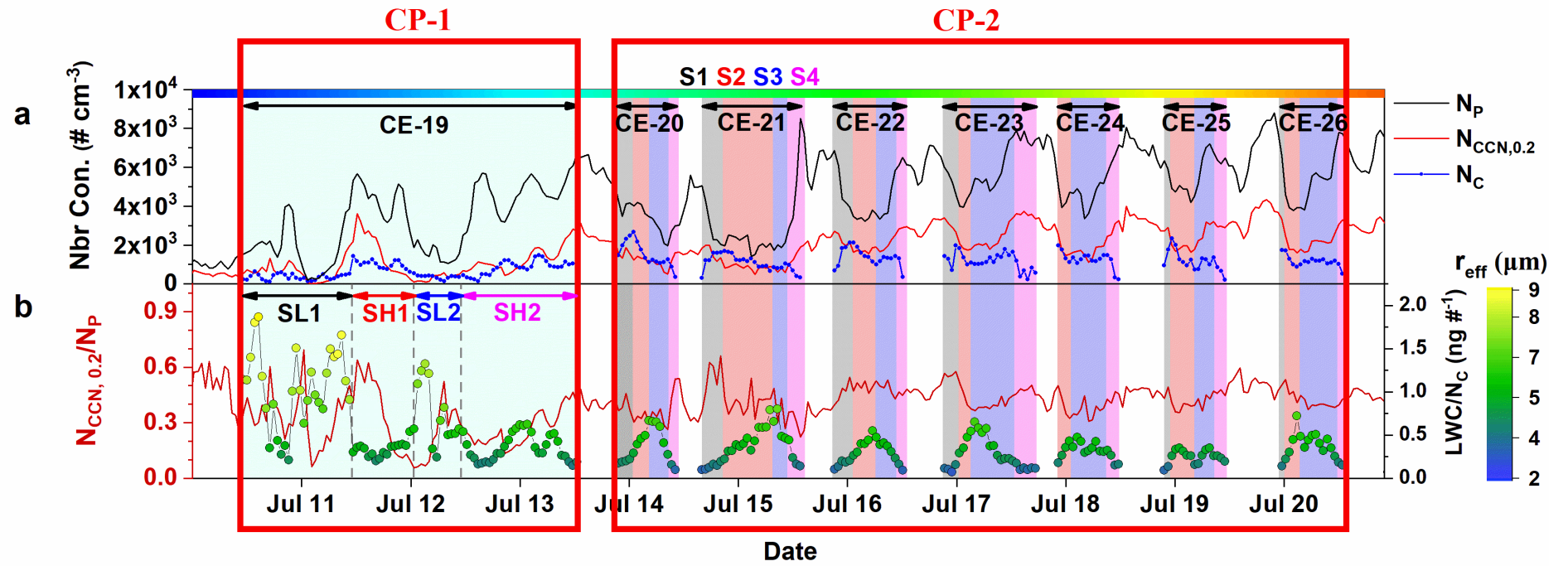
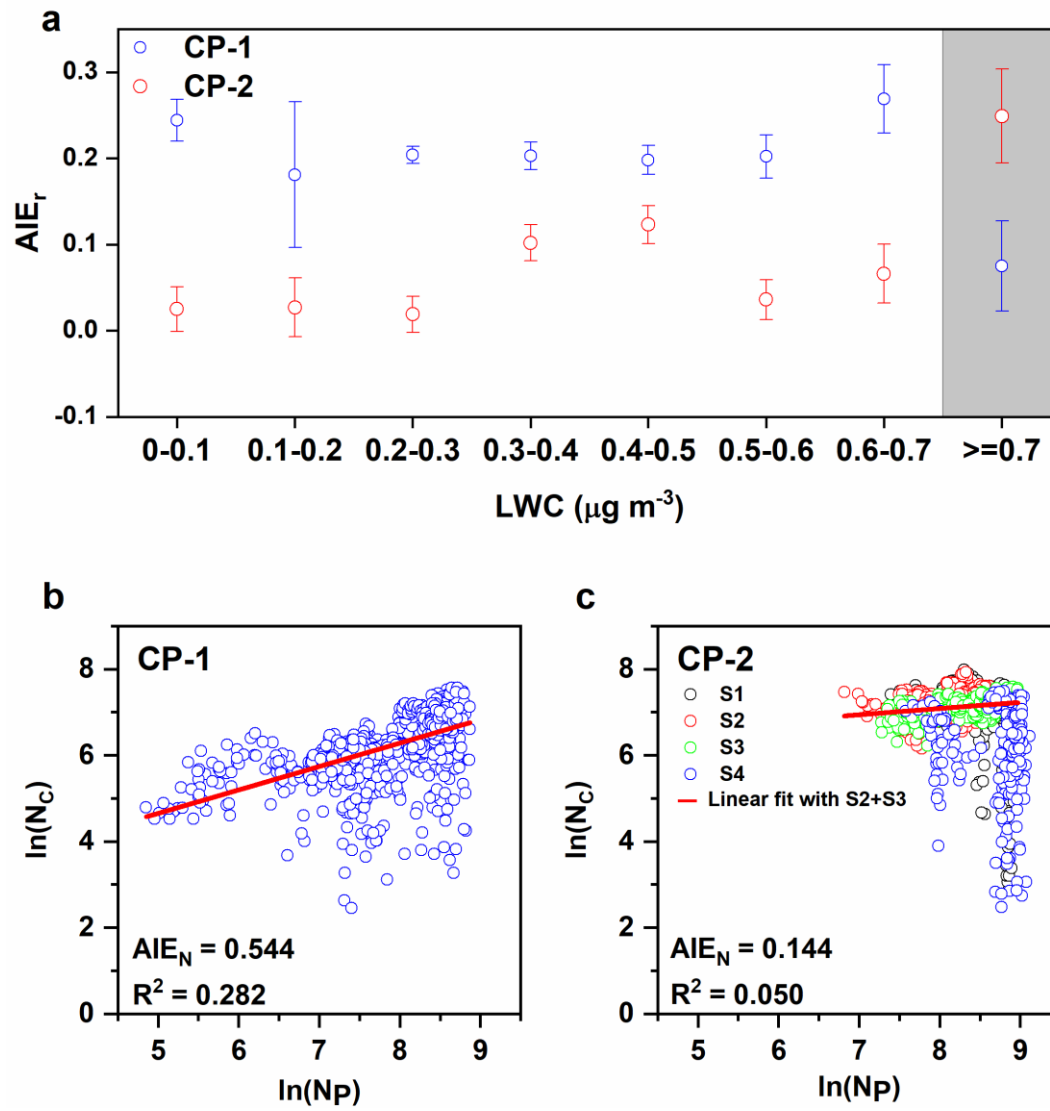


Figure 2: The monitoring information of CP-1 and CP-2. Including (a) Wind speed ( $WS$ ,  $\text{m s}^{-1}$ ) and wind direction ( $WD$ ), (b) cloud based height ( $CBH$ , m) (c) relative humidity ( $RH$ , %), ambient temperature ( $T_a$ ,  $^{\circ}\text{C}$ ) and dew point temperature ( $T_d$ ,  $^{\circ}\text{C}$ ) (d)  $\text{PM}_{2.5}$  mass concentrations ( $\mu\text{g m}^{-3}$ ) and volumn concentration of  $\text{PM}_{0.8}$  ( $10^{-6} \text{ cm}^3 \text{ cm}^{-3}$ ) (e) size distribution of particles (13.6-763.5 nm) and corresponding geometric mean radius ( $GMr_p$ ) (f) size distribution of cloud droplets (2-50  $\mu\text{m}$ ) and corresponding geometric mean radius ( $GMr_c$ ) (g)  $N_c$  and  $LWC$  of cloud droplets.



1  
2 **Figure 3: Variation of (a)  $N_C$ ,  $N_P$  and  $N_{CCN,0.2}$  (b)  $N_{CCN,0.2}/N_P$  and  $LWC/N_C$  during CP-1 and CP-2.**



1

2 **Figure 4:** (a) The determination of  $AIE_r$  for each  $LWC$  bin with  $0.1 \text{ g m}^{-3}$ . The determination of  $AIE_N$  based on  $N_C$  (b)  
 3 during CP-1 and (c) during CP-2.

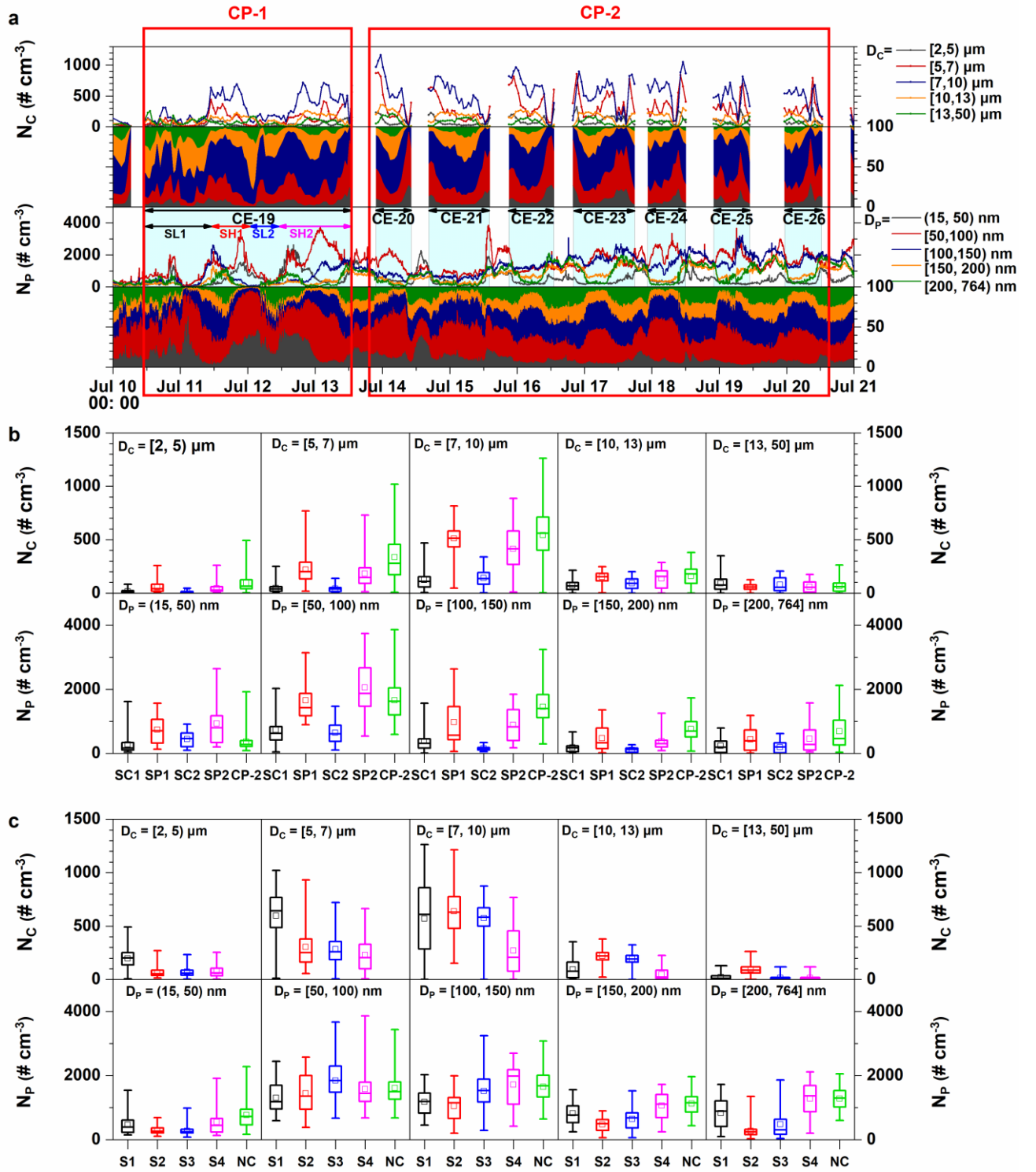


Figure 5: Size distribution of particles and cloud droplets during CP-1 and CP-2. (a) Time series plot of  $N_C$  in five size ranges ( $[2, 5) \mu\text{m}$ ,  $[5, 7) \mu\text{m}$ ,  $[7, 10) \mu\text{m}$ ,  $[10, 13) \mu\text{m}$  and  $[13, 50) \mu\text{m}$ ) and  $N_P$  in five size ranges ( $(15, 50) \text{ nm}$ ,  $[50, 100) \text{ nm}$ ,  $[100, 150) \text{ nm}$ ,  $[150, 200) \text{ nm}$ ,  $[200, 765) \text{ nm}$ ). (b) five size ranges of  $N_C$  and five size ranges of  $N_P$  in SL1, SH1, SL2, SH2 and CP-2 (c) five size ranges of  $N_C$  and five size ranges of  $N_P$  in S1, S2, S3, S4 and NC ("NC" in (c) represents particle size distributions during cloudless period).



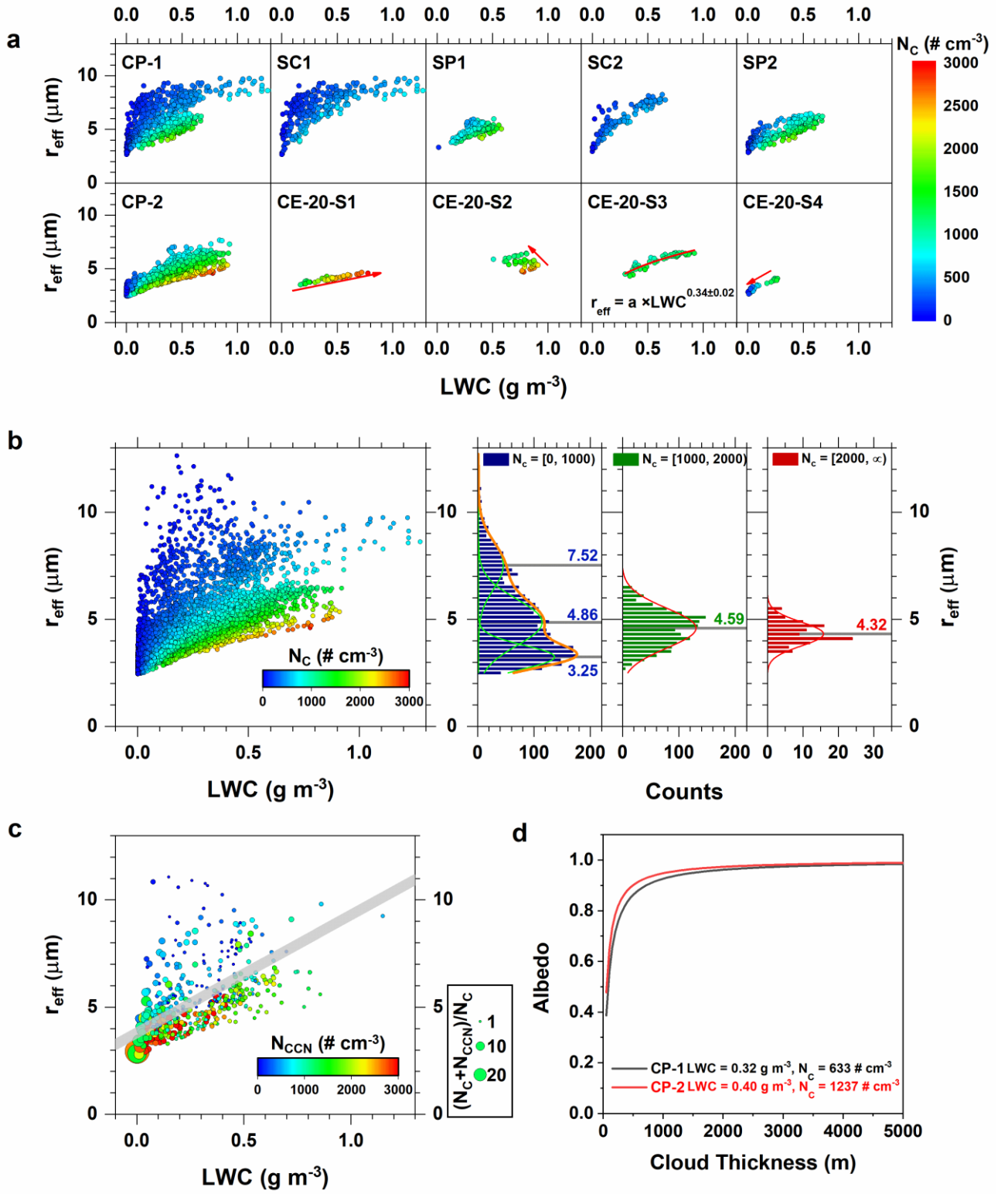


Figure 6: The plot of  $LWC$  versus  $r_{eff}$  (a) in different cloud stages of CP-1 and CP-2 (b) under different  $N_c$  ranges (c) under different  $N_{CCN}$ . The time resolution of the corresponding data was 5 min in (a), (b) and 50 min in (c). (d) The plot of albedo versus the variation of cloud thickness during CP-1 and CP-2. The averaged values of  $LWC$  and  $N_c$  of CP-1 and CP-2 were applied to calculate albedo according to the equations in Section 2.8.